Available online at www.sciencedirect.com

jmr&t Journal of Materials Research and Technology

https://www.journals.elsevier.com/journal-of-materials-research-and-technology

Original Article

Sustainable friction stir spot welding of 6061-T6 aluminium alloy using improved non-dominated sorting teaching learning algorithm

S. Suresh[a], Natarajan Elango[b,*], K. Venkatesan[c], Wei Hong Lim[b], K. Palanikumar[d], S. Rajesh[e]

[a] Department of Mechanical Engineering, Jayalakshmi Institute of Technology, India
[b] Faculty of Engineering, UCSI University, Kuala Lumpur, Malaysia
[c] Department of Metallurgical Engineering, Government College of Engineering, Salem, India
[d] Department of Mechanical Engineering, Sri Sai Ram Institute of Technology, Chennai, India
[e] Department of Mechanical Engineering, Knowledge Institute of Technology, Salem, India

ARTICLE INFO

Article history:
Received 3 June 2020
Accepted 10 August 2020

Keywords:
Swept friction stir spot welding
Aluminium alloy
Nanoparticles
Non-dominated sorting teaching learning based optimization
Lap shear load
Wear

ABSTRACT

Swept Friction Stir Spot Welding is provoked and fascinated for its captive performance in building space frame structures, ship buildings and panels of automotive vehicles. The aim of the current research is to avoid the wastage in welding of 6061-T6 aluminium alloy and to improve the sustainabilty of the weld process. Al_2O_3 nanoparticles were added into the guide hole for improving the weld characteristics. The percentage of reinforcement was varied by changing the guide hole diameter as 1.5, 2.0, 2.5 and 3.0 mm. An improved NSTLBO algorithm was proposed and applied. The proposed algorithm predicted the optimum welding parameters as D = 2.8 mm, N = 1387 rpm and F = 17 mm/minute with the predicted wear, lap shear load and microhardness of 197 microns, 6134 N and 94.6 HV, respectively. The validation experiments were further done and the error within 0.5% was found between the actual and predicted results. The results of proposed algorithm was evaluated with other popular meta-heuristic algorithms for the effectiveness. The microscopic examinations on weld zones and fracturerd samples were also presented. Industries can use these best process parameters predicted by the proposed algorithm for earning the best weld characteristics from eco-friendly welding.

1. Introduction

The ultimate aim of the designers is to choose the appropriate material and dimensions for their components. The aluminium alloys or magnesium alloys are preferred for the parts of automotive and aerospace for the reason of reducing mass moment of inertia [1]. The joining process is regarded as a predominant method in most of the assembly of parts. Since the aluminium alloy has lower tensile strength than steel, it is relatively difficult to join the aluminium alloy parts by fusion welding. It gets a tougher oxidized layer during the welding and takes impurities in its molten state and subsequently ends up with weak and porous welds. Solid state joining methods are largely preferred for joining the frame

* Corresponding author.
E-mail: cad.elango.n@gmail.com (N. Elango).
https://doi.org/10.1016/j.jmrt.2020.08.043

parts of the vehicle. Friction Stir Spot Welding (FSSW) is an eco-friendly welding that collectively preferred for producing spot joint on aluminium alloys. FSSW may result the weld with no contamination, blowholes, porosity and cracks. In FSSW, a non-consumable tool is rotated and pressed with a high force against top surface of two overlapping sheets. The frictional heat and the applied pressure bonds the components metallurgically without melting. The tool is drawn out of the workpiece after a dwell time. Iwashuta [2] discussed about FSSW of lightweight aluminium automobile bodies. Ojo et al. [3] reviewed FSSW of aluminium alloys. Haghshenas and Gerlich [4] reviewed joining of automotive sheet materials by FSSW method. Burford et al. [5] studied the rate of fatigue crack growth on FSSW weld joints and rivet joints and reported that swept FSSW produces favourable residual stresses that assist in decreasing the crack growth rate along the joint line. The quality of frictional weld joints depends on many process parameters such as rotational speed of the tool, rate of tool plunge, depth of shoulder plunge, dwell time, length of tool pin, pin profile and tool shoulder. These factors affect the mechanical properties and metallurgical behavior of the weld joint. A good amount of researches related to the influence of process parameters and weld quality have been conducted in last few decades on conventional FSSW [6–10].

The fillers can be added into the guide hole for improving the weld characteristics. Barmouz et al. [11] reported that the straight cylindrical pin profile of FSSW offers a homogeneous distribution of filler particles in the weld region as compared to square pin profile. Bahrami et al. [12] reported the effect of reinforcement of SiC in FSSW butt joints of AA7075-O for the increase of mechanical properties of the joint. Also reported that the increase of tool rotational speed would give the uniform dispersion of filler in weld region. Tebyani et al. [13] used SiC nanoparticles of 25 nm to produce FSSW joint of interstitial-free steel and reported that the hardness and joint strength were improved significantly compared to SiC free joints. Saeidi et al. [14] discussed the significance of reinforcement of ceramic particles in FSSW joints for the improvement of wear and corrosion resistance. Wu et al. [15] reported the effect of reinforcement of SiC particles in AZ31 magnesium alloy FSSW joints. Suresh et al. [16] added SiC nanoparticles into the guide hole in FSSW of 6061-T6 aluminum alloy. They investigated the effect of SiC nanoparticles and reported that 29% of filler produces the maximum weld characteristics. Suresh et al. [17] in their another study reported the influence of tool rotational speed in conventional FSSW of Al_2O_3 nanoparticles reinforced 7075-T6 Aluminium alloy.

Su et al. [18] conducted the fatigue study and failure mode analysis on swept friction stir spot weld (SFSSW) of alclad AA2024 sheets. They reported that nugget pullout mode and interfacial mode are two different failure modes observed from cross-tension specimens. Venukumar et al. [19] conducted FSSW and refill FSSW on AA6061-T6 aluminium alloys and observed shear fracture, base material fracture, nugget pull out fracture and circumferential fracture during the examination of joints. They also reported that the initiation of cracks is at the partial bonding region of the weld, irrespective of fracture modes. Suresh et al. [20] evaluated conventional FSSW and SFSSW of6061-T6 aluminium alloy. They observed from the lap shear tests that the conventional FSSW samples fail due to shear fracture, nugget pullout fracture and circumferential fracture, but SFSSW samples fail due to only circumferential fracture. The weld defects and low weld strength are obtained during friction stir welding, if optimum weld parameters are not followed.

Only a few researches have been carried out so far in the area of the effect of process parameters on SFSSW. Brown et al. [21] studied SFSSW of similar materials and dissimilar materials on the anodized AA2219-T6 sheets that are widely used in automobiles and aerospace. They reported that SFSSW is able to produce the mechanical properties similar to riveting. Awang et al. [22] investigated the SFSSW of aluminium alloy and reported that tool travel speed and heat dissipation are significant parameters influencing the strength of the weld joint. Yoon et al. [23] conducted the welding with a new approach similar to SFSSW process for joining Al/Fe dissimilar metals. They reported that the radius of rotation and moving direction of the tool are significant parameters that influence

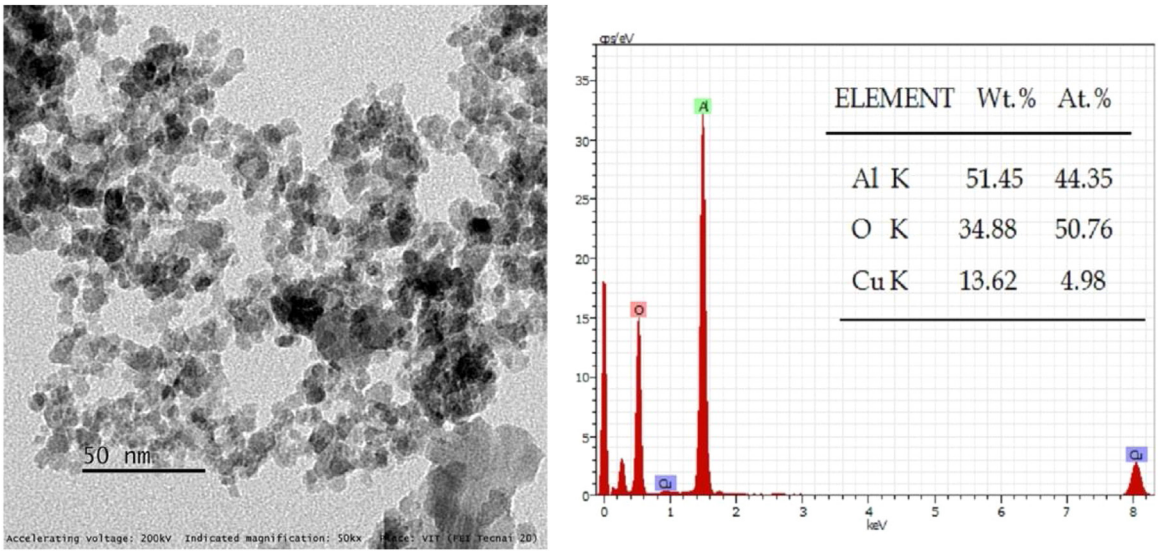

Fig. 1 – TEM-EDS of as received Al_2O_3 nanoparticles.

the width of weld joint and shape of the hook. Huang et al. [24,25] applied a new self-riveting friction stir welding technique to join aluminium alloy and steel and observed the improved weld strength.

The reinforcement of guide hole with appropriate nano fillers do improve the quality of FSSW joints. But substantial research has not been conducted on SFSSW joints, and particularly with reinforcement of guide holes. The investigation on the optimum process parameters will be more supportive for industries working with aluminium alloys in terms of producing high quality SFSSW joints, which, no research has been attempted so far, to the knowledge of authors.

The current research is to optimize process parameters of SFSSW of AA6061-T6 aluminium alloy. The guide hole diameter (D), tool rotational speed (N) and tool traverse speed (F) were considered as independent process parameters to be optimized in order to get the maximum lap shear load (SS), maximum microhardness (MH) and minimum wear (W). The experimental design was conducted in order to design L_{16}orthogonal array. The weld samples were prepared accordingly and the response variables with respect to each experimental run were measured and recorded. Further, Response Surface Model (RSM) representing maximization of lap shear load, maximization of hardness and minimization of wear were developed. A new multi-objective optimization algorithm, an improved version of non-dominated sorting teaching learning based optimization(NSTLBO) was developed and applied. It is with improved learning phases (MLP) of NSTLBO to search for the optimal parameters of the proposed welding model that aims to obtain minimum wear, maximum lap shear load and microhardness simultaneously.

The paper is organized as follows; The materials used in SFSSW, experimental design and the preparation of weld samples are discussed in sections 2.1,2.2 and 2.3 respectively. The mechanical tests and measurement of lap shear load, micro hardness and wear at the weld zone are presented in section 2.4. The development of the new optimization algorithm and simulation are discussed in Section 3. The results of the simulation, validation of the predicted data, performance metrics are presented in Section 4. Lastly in Section 5, the microstructure of the weld samples and defects are shown and discussed.

2. Experimental method and materials

2.1. Materials and preparation of weld samples

The aluminium alloy 6061-T6, being a replacement for steel finds numerous applications in automobile and aircraft industries. AA6061-T6 sheets of 2 mm in thick were purchased from Cluster Trading Corporation, India. The fillers, aluminium oxide (Al_2O_3) nanoparticles with the average particle size of 30 nm were purchased from Hongwu International Group Ltd., China. Transmission Electron microscopic (TEM) image and EDS analysis of Al_2O_3 nanoparticles in as-received condition is shown in Fig. 1. Firstly, the weld coupons of size 100 × 35 mm were prepared from AA6061-T6 alloy through Electrical Discharge Machining.

Machined and hardened H13 steel tool (56–59 HRC) was used in all SFSSW experiments. It provides the sufficient strength, toughness and wear resistant at the welding temperature than the material to be welded [26]. The tool consists of M5 right-handed threaded pin, 12 mm flat shoulder and shank as shown in Fig. 2(a). Based on the thickness of the workpiece and the clearance required between the backing plate and the pin tip, the tool pin length was fixed as 2.85 mm. The features of SFSSW tool is listed in Table 1. The threaded tool pin was used for improving the material flow and for avoiding the formation of voids as reported by Rai et al. [27].

2.2. Design of experiments (DOE)

The weld process parameters such as guide hole diameter (D), tool rotational speed (N) and tool traverse speed (F) were primary independent variables. It is obvious that the volume of nanoparticles reinforcement is directly proportional to the guide hole diameter. Lap shear load, microhardness and wear were considered as dependent variables (response variables) involved in the current SFSSW. A preliminary study

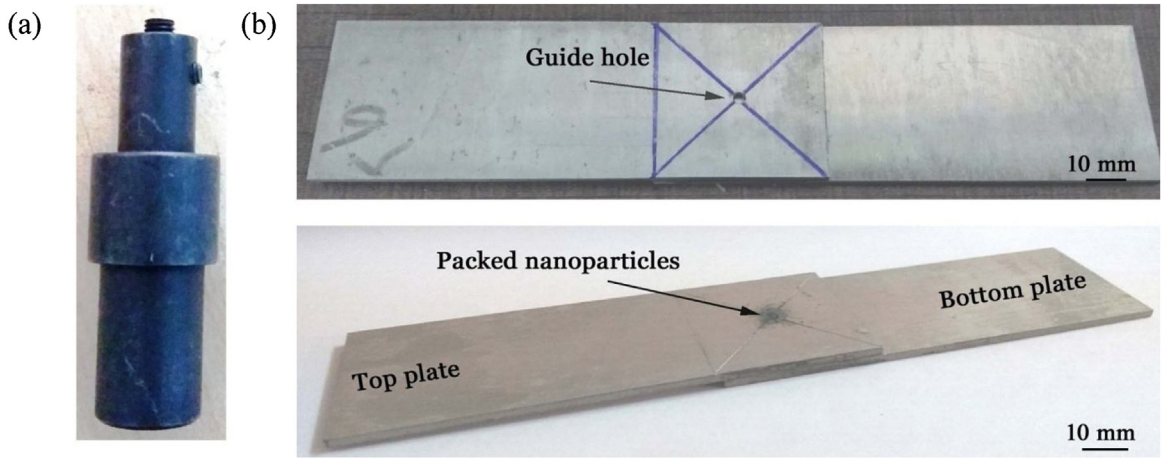

Fig. 2 – (a) SFSSW Tool (b) Location of the guide hole in the base plate and packed nanoparticles in the guide hole before welding.

Table 1 – Features of SFSSW tool.

Tool Material	Tool pin	Shoulder Profile	Tool size (mm)
H13 tool steel	Round with M5 right hand threaded	Flat	Shoulder Diameter:12 Pin Length:2.85 Pin Diameter:5

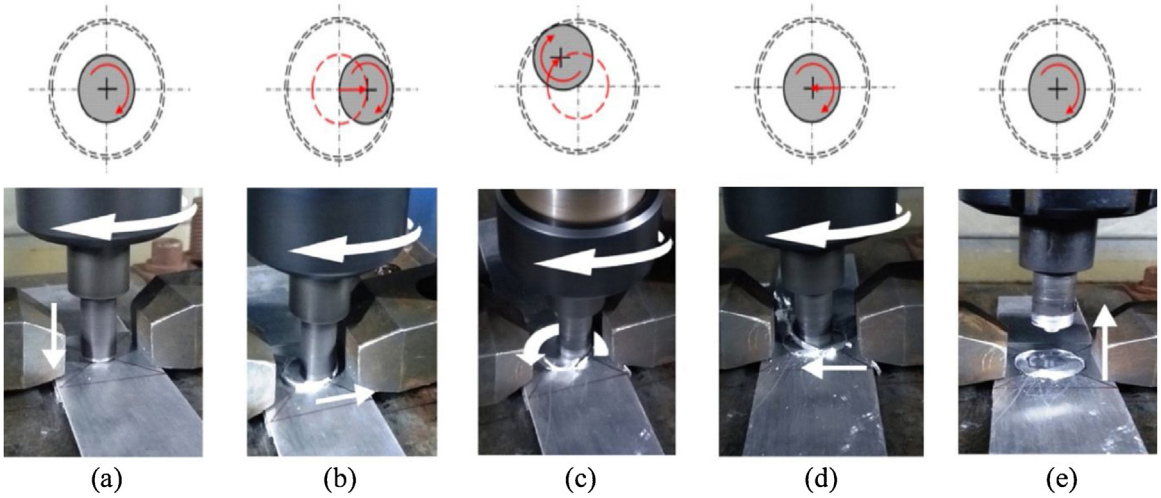

Fig. 3 – Various steps of SFSSW (a) Plunging (b) Outward movement (c) 3600 circular sweeping (d) Inward movement and (e) Retraction of tool.

Table 2 – Details of initial SFSSW trials for setting the range of process parameters.

Parameter	Range	Photograph/Micrograph	Type of defect
Tool rotational speed(N in rpm)	< 1200 rpm and > 1800 rpm		Worm hole
Tool Traverse speed (F in mm/minute)	< 10 mm/minute >25 mm/minute		Surface lack of fill

was initially conducted in order to identify the appropriate range and level of parameters for Design of Experiments (DOE). DOE is a systematic approach to decide the minimum number of experiments to be conducted. Table 2 depicts the defects observed during the experiments during preliminary study.

Some defects were observed when N < 1200 rpm, N > 1800 rpm, F < 10 mm/minute and F > 25 mm/minute. With these observations, the range of process parameters were decided and fixed for further development of DOE. SFSSW process parameters and the respective four levels used in DOE is shown in Table 3. L_{16} orthogonal array represeenting the process condition is shown in Table 4.

2.3. *SFSSW – experimentation*

Before conducting SFSSW, guide hole was prepared on AA6061-T6 weld coupons according to L_{16} orthogonal array. Top and bottom plates were overlapped by 35 mm and Al_2O_3 nanoparticles were packed tightly in the guide hole before the welding is done. A photograph of the position of the guide hole with packed nanoparticles in weld coupon is shown in Fig. 2(b). The SFSSW experiments were carried out using CNC vertical machining center (Make: ACE Micrometric, India). The plates were clamped rigidly in lap configuration using a specially designed fixture and the required clamping was ensured for the better quality welding.

Table 3 – The SFSSW process parameters and their respective levels.

Process parameter	Levels			
	1	2	3	4
Guide hole diameter(D) in mm	1.5	2	2.5	3
Tool rotational speed (N)in rpm	1200	1400	1600	1800
Tool traverse speed(F) in mm/minute	10	15	20	25

Table 4 – L_{16} Orthogonal array.

Experiment no.	Guide hole diameter (D) in mm	Tool rotational speed (N) in rpm	Tool traverse speed (F) in mm/minute
1	1.5	1200	10
2	1.5	1400	15
3	1.5	1600	20
4	1.5	1800	25
5	2.0	1200	15
6	2.0	1400	10
7	2.0	1600	25
8	2.0	1800	20
9	2.5	1200	20
10	2.5	1400	25
11	2.5	1600	10
12	2.5	1800	15
13	3.0	1200	25
14	3.0	1400	20
15	3.0	1600	15
16	3.0	1800	10

Fig. 3 depicts the various steps followed in preparing AA6061-T6/Al_2O_3 SFSSW joints. The weld process was begun with the plunging of the rotating tool in the configured plate to a predetermined plunge depth to achieve the frictional heat beneath the shoulder and around the tool pin (Fig. 3a). The tool was then moved linearly outwards for a distance of 2.5 mm (Fig. 3b). When the tool started moving in a circular path for 360° around the tool plunge center for an additional stirring action (Fig. 3c), the tool was moved to weld center to complete the stirring action (Fig. 3d). Finally, the tool was retracted from the weld area (Fig. 3e). The CNC program was developed in order to carry out the above operations, hence, the consistency and reliability of the experimental runs were ensured. The photograph of weld samples is shown in Fig. 4.

Fig. 4 – Photograph of AA6061-T6/Al_2O_3 SFSS Welded samples.

2.4. *Mechanical tests – measurement of response parameters*

As discussed in the previous section, weld samples as shown in Fig. 4 were prepared as per the AWS-D 17.2standard [28] for lap shear tensile test. Lap shear load of the weld samples was measured using Computerized Universal Testing Machine (Model: TE-JINAN-WDW100). The tensile load was applied at 1 mm/minute and the maximum load at which the sample fractured was noted. Five samples were tested at room temperature and the mean of the measurement was considered as the lap shear load of the SFSSW weld.

The micro hardness of the weld samples was measured using Vicker's microhardness testing apparatus (Model: Wilson Hardness-402 MVD). The force of 1 kg with a dwell time of 20 s was applied for measuring microhardness at the cross section of the welded samples shown in Fig. 5a. The same procedure was followed for five different welded samples and the mean of the measurement was considered as the microhardness of the SFSSW.

The dry sliding wear test as per ASTM G99 standard at room temperature was conducted using Pin-On-Disc wear test apparatus (Ducom TR20). The specimens in 4 mm diameter and 30 mm height were prepared from the stir zone(SZ) of cross-sectioned welded samples as shown in Fig. 5(b). All the prepared specimens were set to press against an EN32 die steel disc to slide on the Pin-On-Disc apparatus. The sliding speed of 2 m/second, normal load of 20 N and sliding distance of 1000 m were kept constant throughout the experiments. The wear

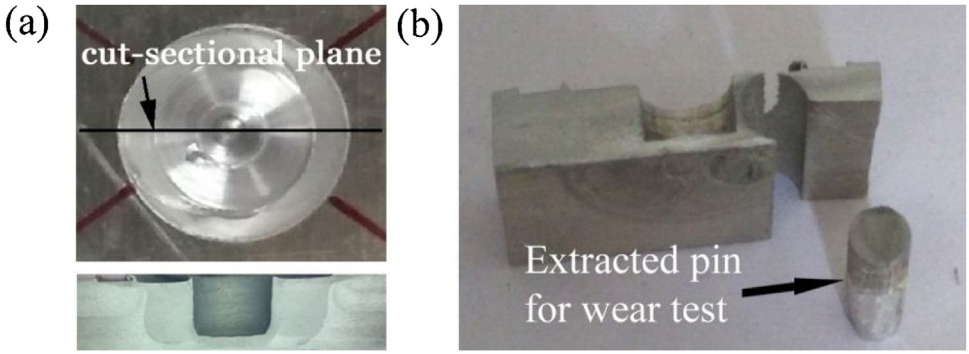

Fig. 5 – (a) Cross-sectioned sample used in microhardness test (b) Sample used in wear test.

parameters were measured for five different samples and the mean of the measurements was computed.

Table 5 shows the mean value of lap shear load, hardness and wear with respective to each experimental run. All these measured data along with their respective control parameters were considered further to develop the model for the optimization. The model development and simulation is discussed in section 3.

3. Model development and proposed optimization algorithm

3.1. *Regression model*

Regression is a modelling approach widely used in describing the output of a complex process through the formulation of nonlinear functions by considering several input process parameters with boundary limits. Different optimization methods are generally applied to solve these regression models in order to obtain the best combinations of parameter settings that can lead to the optimal performance of processes.

In order to optimize the control parameters for maximizing or minimizing of response variable, the respective optimization function is to be derived. The experimental data as listed in Table 6 was used to derive the following regression equations (Eq. 1–3) for lap shear load (*SS*), microhardness (*MH*) and wear (*W*). The Eq. (1) and (2) are maximization functions, as the shear load and microhardness are to be maximised. Eq. (3) is a minimization function as wear is to be minimized.

$$SS = -1297 + 3106D + 4.12N + 23.6F - 558.0DxD - 0.001118NxN - 1.072FxF - 0.201DxN + 8.91DxF - 0.0084NxF \quad (1)$$

$$MH = -25.6 + 47.01D + 0.0587N + 2.088F - 6.262DxD - 0.000007NxN - 0.00732FxF - 0.00804DxN - 0.182DxF - 0.001016NxF \quad (2)$$

$$W = 195.6 - 23.6D + 0.0590N + 1.42F + 7.00DxD - 0.000013NxN + 0.0200FxF - 0.00795DxN - 0.727DxF - 0.000386NxF \quad (3)$$

In the past, numerous mathematical programing methods such as the nonlinear programing, dynamics programming, quadratic programming etc. were used as the popular methods to solve these optimization models. However, these conventional approaches tend to obtain the sub-optimal or even not optimal solutions due to the poor guess of initial solutions [29]. Recently, the emergence of nature-inspired based optimization algorithms is deemed as the promising solution to overcome the aforementioned challenges. In contrary with mathematical programming approaches, the nature-inspired optimization algorithms are able to converge efficiently towards the near-optimal solutions without requiring the precise gradient information of objective functions. Hence, numerous real-world engineering optimization problems were solved successfully with nature-inspired algorithms [30–36]. The optimization of machining or manufacturing problems involve more than one independent variables (also called control parameters or process parameters) and one or more than one response parameter. The fine-tuning of multiple input process parameters of any given manufacturing problem can be conducted through nature-inspired algorithms. Both priori and posterior methods are popular in nature-inspired algorithms for solving multi objective problems. The priori method can produce only one optimum solution in each run of simulation. On the other hand, the posterior method can generate a complete set of trade-off solutions in a single run of simulation. It is deemed as a more competitive approach in addressing the frequent changes of customer requirements. The process planner can select a preferred optimum solution from these solution sets by using different performance selection index method in response to the latest requirements specified by other stakeholders.

A significant amount of studies have been conducted in the past to address the multi-objective manufacturing prob-

Table 5 – Response parameters of AA6061-T6/Al_2O_3 SFSSW joints.

Experiment No.	Control parameters			Response parameters		
	Guide hole diameter (*D* in mm)	Tool rotational speed (*N* in rpm)	Tool traverse speed (*F* in mm/minute)	Lap shear Load (*SS* in Newton)	Microhardness (*MH* in HV)	Wear (*W* in Microns)
1	1.5	1200	10	5278	82	214
2	1.5	1400	15	5349	86	218
3	1.5	1600	20	5551	89	224
4	1.5	1800	25	5249	85.7	223
5	2.0	1200	15	5714	90	210
6	2.0	1400	10	5908	91.2	212
7	2.0	1600	25	5669	91.8	213
8	2.0	1800	20	5817	93.5	206
9	2.5	1200	20	6148	94.7	193
10	2.5	1400	25	6087	93.5	197
11	2.5	1600	10	6124	96.1	200
12	2.5	1800	15	6134	91.5	200
13	3.0	1200	25	5923	95.1	195
14	3.0	1400	20	6002	92.1	197
15	3.0	1600	15	6103	97	194
16	3.0	1800	10	5912	94.9	198

Table 6 – Comparison between the predicted and experimental values.

Welding parameter	Predicted results$w_1 = w_2 = w_3 = 1/3$	Validation experimental result	Error rate
Guide hole diameter, *D* (mm)	2.8	Use of the same predicted process parameters	
Total rotational speed, *N* (rpm)	1387		
Total traverse speed, *F* (mm/min)	17		
Lap shear load (N)	6134	6145	0.179 %
Microhardness (HV)	94.6	94.3	0.317 %
Wear (Microns)	197	196	0.507 %

lems. The feasibilities of multi-objective versions of Cuckoo search optimization and Jaya algorithm in addressing both conventional and modern machining processes were investigated and reviewed in [37–40]. These studies include various processes such as drilling, grinding, ultrasonic machining, abrasive water jet machining, electrochemical machining (ECM), electric discharge machining (EDM), laser cutting, and ion beam micro-milling.

The process parameters of micro-EDM of Stainless Steel 316 L were fine-tuned and optimized by Suresh et al. [41]. The almost similar approach was followed by Sathiyamoorthy et al. [42,43] for optimizing process parameters of ECM of die tool steel and AISI 2020 Austenitic stainless steel respectively. Teimouri et al. [44] performed multi-objective optimization of process parameters of ultrasonic machining using imperialist competitive algorithm. Mohanty et al. [45] performed tuning of process parameter of EDM using particle swarm optimization(PSO). Ong et al. [46] formulated a multi-objective EDM of polycrystalline diamond tool and carried out the optimization using neural network. Nagarajan et al. [47] conducted multiobjective optimization of parameters in dry EDM of LM13 aluminium alloy. Kaviarasan et al. [48] optimized spindle speed, feed rate, and tool point angle during drilling of Delrin material using ANN.

Different enhanced versions of TLBO have been recently emerged as popular nature-inspired search algorithms to solve various types of multi-response optimization of manufacturing problems, because these approaches require less intensive efforts in tuning the algorithm-specific parameters. The minimization of carbon emission and operation time during turning operations was carried out using TLBO by Lin et al. [49]. Abhishek et al. [50] developed a nonlinear regression model to represent the machining of a carbon fiber reinforced polymer composite and aimed to achieve maximum cutting force, surface finish and material removal rate through priori method of TLBO. Rao et al. [51] proposed a modified TLBO known as non-dominated sorting TLBO (NSTLBO) to solve numerous machining problems known as ECM, wire-EDM, ion beam micro-milling and laser cutting. Natarajan et al. [52,53] conducted multi-objective optimization of machining of Delrin and polytetrafluoroethylene (PTFE) materials using enhanced multi-objective TLBO (EMTLBO).

A new improved version of TLBO, namely Non-Dominated Sorting Teaching Learning Based Optimization with Modified Learning Phases (NSTLBO-MLPs) was proposed and implemented in the current research for optimizing the SFSSW process parameters. It is to search for the optimal parameters of the proposed welding model that can lead to the minimization of wear, maximization of lap shear load and maximization of stir zone microhardness simultaneously. Some notable modifications were incorporated in the algorithm by refining its algorithmic framework in order to enhance the search performance of NSTLBO-MLPs and enable it to provide more accurate representation of real-world teaching and learning paradigm. Referring to the metric of Euclidean distance, a modified selection scheme for teacher was incorporated into NSTLBO-MLPs. A new computation method was also introduced to assign the unique mean position of each learner

based on social learning mechanism. These enhanced the exploitation search of algorithm while preserving the population diversity. Meanwhile, two search operators with different exploration and exploitation strengths, namely independent learning and adaptive peer learning mechanisms were introduced into the modified peer learner phase of NSTLBO-MLPs. These facilitate the different needs of learners to update their knowledge in classroom. Considering the relative level of importance of all objective functions that change dynamically, a fuzzy decision maker was also employed in determining the most appropriate welding parameters from the Pareto front generated.

3.2. *Teaching-learning-Based optimization*

The search mechanism of TLBO was motivated by teaching and learning paradigms of conventional classroom. Suppose that N refers to the population size of TLBO. The initial population of TLBO learner are randomly generated at the beginning stage of search process. Let $X_n = \left[X_{n,1}, ..., X_{n,d}, ..., X_{n,D}\right]$ be the candidate solution represented by each n-th learner to solve an optimization problem with D dimensional size, where $d \in [1, D]$ is the dimension index. An objective function $\Psi(X_n)$ is defined to quantify the knowledge or competency level of each n-th TLBO learner, where the value of $\Psi(X_n)$ can be improved further through the teacher phase and/or learner phases described as below.

All TLBO learners are envisioned to update their knowledge or competency level during the teacher phase by interacting with the best learner in population, i.e., the teacher solution represented with $X^{teacher}$, while taking the mainstream knowledge of population into account. For conventional TLBO, the mainstream knowledge of population is quantified via the mean position value of X^{mean} computed as follow:

$$X^{mean} = \frac{1}{N}\sum_{n=1}^{N} X_n \tag{4}$$

Suppose that r_1 is a random number between zero and one, T_f is a teaching factor with the integer value of 1 or 2 for indicating the influences of population's mainstream knowledge X^{mean}. Let X_n^{new} be the new solution of the i-th learner that can be obtained from teacher phase, then:

$$X_n^{new} = X_n + r_1\left(X^{teacher} - T_f X^{mean}\right) \tag{5}$$

After completing the teacher phase, every learner can start interacting with other population members in the subsequent learner phase to update its knowledge level in terms of fitness. Each of the n-th learner can randomly select a peer with the learner index of s from the population for the peer learning process. Depending on the fitness value of randomly selected s-th peer, two possible scenarios of peer learning can be anticipated. Firstly, the n-th learner tends to approach towards and learn from its s-th peer if the latter solution is found to be superior than the former one as indicated in Eq. (6). Secondly, the randomly selected s-th peer learner becomes a source of repulsion to discourage the convergence of n-th learner towards it if X_s has worse fitness than X_n as shown in Eq. (7):

$$X_n^{new} = X_n + r_2\left(X_s - X_n\right) \tag{6}$$

$$X_n^{new} = X_n + r_2\left(X_n - X_s\right) \tag{7}$$

where r_2 is a random number between 0–1.

For each n-th learner, the original solution X_n can be replaced by the new solution X_n^{new} obtained from the teacher or learner phases if X_n^{new} is found to have more promising fitness than X_n. Otherwise, the inferior X_n^{new} is to be discarded. The knowledge enhancement of each learner is performed iteratively using Eqs. (4) to (7) until the termination conditions of TLBO are met. At the end of search process, the best solution found by TBLO so far, i.e., $X^{teacher}$ is used to solve the given optimization problem. The following sections present the modifications introduced in the proposed algorithm and the respective results.

3.3. *Proposed modified learning phases of TLBO*

For most TLBO variants, certain search mechanisms adopted in their frame works might not accurately reflect the actual scenario of teaching and learning paradigms in classroom. These deviations tend to restrict the abilities of these TLBO variants in balancing the exploration and exploitation searches, as well as their robustness in solving the optimization problems with different fitness landscapes. In order to overcome these challenges, an improved version of posterior approach, namely the NSTLBO-MLPs was proposed.

The search mechanisms incorporated into both teacher and learner phases of NSTLBO-MLPs were further refined in order to ensure the algorithmic framework can represent the actual teaching and learning process in classroom more accurately, leading to improved search performance of algorithm. Furthermore, fast non-dominated sorting (FNDS) and crowding distance (CD) were included as essential components of the proposed algorithm for handling multi-objective optimization problems (MOPs).

3.3.1. *Overview of dominance and pareto optimality*

Consider a MOP with the total number of M objectives and each learner X_n produces an objective function value denoted as $\Psi_m(X_n)$ in solving the m-th objective, where $m = 1,\ldots, M$ and $n = 1, \ldots, N$. Unlike the optimization problems with single objective where the quality of all solutions can be easily distinguished, it is challenging to rank all solutions of MOPs based on to their objective function values because of the presence of multiple contradictory objective functions. Pareto dominance concept was therefore used to solve these challenges with some related definitions as provided below:

Definition 1. . A solution X_n dominates another solution X_s if the former solution shows the better or same performances for all objectives considered and outperforms the latter solution for at least one objective. Mathematically, $X_n \succ X_s$ if and only if $\Psi_i(X_n) \leq \Psi_i(X_s)$ for $\forall i \in \{1, 2, ..., M\}$ and $\Psi_j(X_n) < \Psi_j(X_s)$ for $\exists j \in \{1, 2, ..., M\}$ or vice versa.

Definition 2. . Pareto optimal solution X^* can be identified if none of the other solution X found can dominate X^*, i.e., $X^* \succ X$. A Pareto optimal set can then be formulated by considering these collection of Pareto optimal solutions.

Definition 3. . Pareto front can be obtained by mapping all solution members stored in the Pareto optimal set to objective function space.

3.3.2. *Introduction of essential mechanisms (FNDS and CD)*

In order to solve a given MOP successfully, the capability of NSTLBO-MLPs in generating the evenly distributed Pareto fronts is essential. Initially, a NSTLBO-MLPs population consisting of N learners, represented using $\boldsymbol{P} = [X_1, ..., X_n, ..., X_N]$, was randomly initialized. Two essential mechanisms known as FNDS and CD were employed to rank the quality of solution of all NSTLBO-MLPs learners. FNDS metric ensures that the useful information contained in all non-dominated solutions are leveraged to adjust the paths of all learners and to ensure that they are moving towards the promising regions of search space, hence obtaining the approximated Pareto fronts that are close to the actual Pareto front. The solution diversity within a Pareto front can be preserved through the computation of CD metric. Generally, a non-dominated solution with larger CD values (i.e., less occupied) has higher likelihood to be selected in assisting the search process of other NSTLBO-MLPs learners.

For FNDS, each n-th learner X_n consists of two entities are to be determined, namely (i) domination count C_n to indicate the frequency of X_n being dominated by other solutions and (ii)set S_n to memorize all solutions that are dominated by X_n. During the first round of sorting process, Pareto dominance is employed to identify all non-dominated solutions with $C_n = 0$ and these solutions are then assigned into the first level of Pareto front F_1.For each n-th learner with $C_n = 0$ is stored into F_1, each s-th learner X_s contained in the set S_n is visited once and the associated domination count C_s is deducted by one. In order to construct the second level of Pareto front denoted as F_2, another list variable Q is defined to store all s-th learner with the updated domination count of $C_s = 0$. Similar procedures are performed on Q to iteratively construct the remaining levels of Pareto fronts that are represented as $F_3, ..., F_R$, where R is the upper limit of Pareto front level. As shown in Fig. 6, the FNSD procedure is repeated until the Pareto rank and Pareto front layers of all NSTLBO-MPLs learners, represented using the sets of $\boldsymbol{Rank} = [Rank_1, ..., Rank_n, ..., Rank_N]$ and $\boldsymbol{F} = [F_1, ..., F_r, ..., F_R]$, respectively, are obtained. Note that the parameter r represents the index of a given Pareto front level.

Meanwhile, the premature convergence of NSMTLBO-MLPs can be addressed by leveraging the concept of CD to preserve the solution diversity in Pareto front. Suppose that the closeness of each n-th learner can be quantified using a metric defined as Δ_n. Mathematically, the value of Δ_n can be obtained by measuring the average distance between two closest neighbors of X_n for all M objective functions. Consider $|F_r|$ as the total solution members contained in each r-th Pareto front level, while the initial CD value of the a-th solution in each r-th front is $\Delta_{a,r} = 0$, where $a = 1, ..., |F_r|$. Referring to the objective function values obtained in each m-th objective, all solutions assigned in the r-th Pareto front level are sorted and stored into a list defined as $L_{m,r}$. For each m-th objective, assume that each a-th solution belongs to the r-th Pareto front level is sorted to become $L_{m,r[j]}$, i.e., the j-th element of $L_{m,r}$, where $j = 1, ..., |F_r|$. Suppose that $\Psi_m\left(X_{L_{m,r[j]}}\right)$ represents the objective function value obtained by the j-th element of $L_{m,r}$. Then, the corresponding CD value for each j-th sorted member in $L_{m,r}$ is obtained as:

$$\Delta_{L_{m,r[j]}} = \begin{cases} \infty, \text{if} j = 1 \text{or} j = |F_r| \\ \Delta_{L_{m,r[j]}} + \dfrac{\Psi_m\left(X_{L_{m.r[j+1]}}\right) - \Psi_m\left(X_{L_{m.r[j-1]}}\right)}{\Psi_m\left(X_{L_{m.r[|Fr|]}}\right) - \Psi_m\left(X_{L_{m.r[1]}}\right)} \\ if\ j = 2, ..., (|F_r| - 1) \end{cases} \tag{8}$$

As shown in Eq. (8), the infinite crowding distance values are assigned to the boundary solution members of $L_{m,r}$. For each r-th front level, the solution members located in more sparse regions of m-th objective space tends to have larger CD values than those in crowded regions. Same computation procedures are repeated for all R Pareto front levels and all M objective functions as depicted in Fig. 7. Finally, the overall CD value of each n-th learner is determined by summing up the individual CD value associated with each m-th objective function value and represented in a set denoted as $\boldsymbol{\Delta} = [\Delta_1, ..., \Delta_n, ..., \Delta_N]$.

Suppose that $\prec_{cco}$ is a crowding-comparison operator that has crucial role in distinguishing the quality of different solutions of MOPs. Let the Pareto ranks of the n-th learner and s-th learner in NSTLBO-MLPs population are denoted as $Rank_n$ and $Rank_s$, respectively. Referring to Eq. (9),X_n is superior than X_s if $Rank_n$ is smaller than $Rank_s$. For the case of both learners assigned with same Pareto rank, the learner with larger CD is desirable.

$$X_n \prec_{cco} X_s, \text{ if } (Rank_n < Rank_s) \text{ or } (Rank_n = Rank_s) \text{ and } (\Delta_n > \Delta_s) \tag{9}$$

As shown in Eq. (9), crowding-comparison operator was employed to sort all NSTLBO-MLPs learners in the ascending order according to their respective Pareto rank and CD values. Particularly, smaller index value of n was assigned to the learner X_n with smaller $Rank_n$ and/or larger values Δ_n and vice versa.

3.3.3. *Modified teacher phase of NSTLBO-MLPs*

From Eq. (5), each n-th TLBO learner updates its position X_n in teacher phase by referring to the teacher and mainstream knowledge of population denoted as $X^{teacher}$ and X^{mean}, respectively. While it is intuitive to identify the fittest learner as teacher in single-objective optimization problems (SOPs), teacher selection mechanism of MOPs remains as an open-ended challenge because thepresence of multiple conflicting objective functions can generate more than one non-dominated solution that are equally eligible to serve as the source of influence in adjusting the trajectories of all learners.

```
for n = 1 to N do
    for s = n +1 to N do
        if X_n ≻ X_s then                          /*X_n dominates X_s*/
            C_s ← C_s +1;                          /*Update the domination count of X_s*/
            S_n ← S_n ∪ {X_S};                     /*IncludeX_s to the solution set S_n*/
else                                               /*X_s dominates X_n*/
            C_n ← C_n +1;                          /*Update the domination count of X_s*/
            S_s ← S_s ∪ {X_n};                     /*IncludeX_n to the solution set S_s*/
        end if
    end for
    if C_n is equal to 0 then                      /*X_nis not dominated by any learners*/
        Rank_n = 1;                                /*Assign the Pareto rank of X_n*/
        F_1 ← F_1 ∪ {X_n};                         /*Include X_nto the first level of Pareto front*/
    end if
end for
r = 1;                                             /*Initialize the Pareto front level*/
while F_r ≠ ∅ do
        Q = ∅ ;                                    /*Clear the list Q*/
        for n = 1 to |F_r| do                      /*|F_r| = number of elements in F_r*/
            for s = 1 to |S_n| do                  /*|S_n| = number of elements in S_n*/
                C_s ← C_s −1;                      /*Deduct the domination count of X_s*/
                if C_s is equal to 0 then
                    Rank_s ← r+1;                  /*Assign the Pareto rank of X_s*/
                    Q ← Q ∪ {X_S};                 /*Stored X_s into the next level of Pareto front*/
                end if
            end for
        end for
        r ← r +1;                                  /*Update the index of Pareto front level*/
        F_r ← Q;                                   /*Update the next level of Pareto front*/
end while
```

Fig. 6 – Pseudo-code used to summarize the FNDS procedure.

```
Algorithm 2: Δ = Crowding_Distance_Calculation (F)
Determine total Pareto front levels from F as Rand total solution members stored in each r-th front as |F_r|;
for r = 1 to R do
    for m = 1 to M do
        Sort all solution members of r-th front level ascendingly based on the m-th objective function value.
Then, store each j-th sorted member into the list of L_{m,r} and represent it as L_{m,r}[j];
        for j = 1 to |F_r| do
            Calculate the crowding distance of each j-th sorted member in L_{m,r} with Eq. (5);
        end for
    end for
    for a = 1 to |F_r| do
Determine the overall crowding distance Δ_{a,r} of each a-th solution member by summing up the total
individual distance values obtained from all M objective functions;
        Identify the n-th learner associated to the a-th member stored in the r-th front and then assign the
crowding distance of Δ_n as Δ_{a,r};
    end for
end for
```

Fig. 7 – Pseudo-code used to calculate the CD values of all NSTLBO-MLPs learners.

A modified teacher selection mechanism is envisioned to tackle MOPs by effectively utilizing the useful information of all non-dominated solutions assigned to the first level of Pareto front F_1. Instead of assigning the same teacher to guide all learners as in TLBO, the modified teacher phase of NSTLBO-MLPs leverages the expertise of multiple teachers to achieve knowledge enhancement. This can be achieved by allocating the nearest member in F_1 to become the teacher for the n-th

learner. Suppose that $|F_1|$ refers to the total number of elements in F_1 that are eligible to be candidate teachers. Define $X_{a,d}^{Cand}$ as the d-th component of the a-th candidate teacher, while the same dimensional component of n-th learner is represented as $X_{n,d}$ for $a = 1, ..., |F_1|$ and $n = 1, ..., N$. Then, a parameter $E_{n,a}$ is used to measure the normalized Euclidean distance between each n-th learner and the a-th candidate teacher as:

$$E_{n,a} = \sqrt{\sum_{d=1}^{D} \left(\frac{X_{a,d}^{Cand} - X_{n,d}}{X_d^U - X_d^L} \right)^2} \tag{10}$$

Where D refers to the total numbers of decision variable considered. X_d^U and X_d^L are upper and lower limits of variables, respectively in each d-th dimension of $d = 1, ..., D$. Referring to all $E_{n,a}$ values obtained for $n = 1, ..., N$ and $a = 1, ..., |F_1|$ using Eq. (10), the nearest candidate teacher with smallest value of $E_{n,a}$ is then selected to become the teacher $X_n^{teacher}$ of n-th learner in modified teacher phase. Fig. 8 summarizes the procedure used to assign a unique teacher to guide the search process of each NSTLBO-MLP learner as an initiative to enhance the solution diversity in Pareto front. This strategy enables all learners to have opportunity in exploring different promising regions of search space during the optimization process by referring to the locations of their teachers.

Apart from teacher selection mechanism, another issues to be considered in modifying the teacher phase of NSTLBO-MLPs are the modelling of classroom's mainstream knowledge and learning strategy adopted for enhancing the knowledge levels of all learners. For conventional TLBO, the mainstream knowledge is represented by the mean position X^{mean} of all population members as shown in Eq. (1). Nevertheless, this representation might not truly reflect real-world teaching and learning paradigm because each learner might have different perceptions on the mainstream knowledge of classroom, thus different mean positions should be formulated as a unique source of influence for each learner. In addition, the same direction information obtained from $X^{teacher}$ and X^{mean} are utilized to guide the TLBO learner during the teacher phase according to Eq. (2). If the teacher solution with the best performance so far is stagnated into the inferior solution regions of complex optimization problems, the remaining learners have high tendency to be misled by these same $X^{teacher}$ and X^{mean}, then congregate around the similar solution space regions and delivers poor optimization results.

In view of the aforementioned drawbacks, a social learning concept is incorporated to derive the unique mean position for each NSTLBO-MLPs learner. Generally, social learning enables each individual to learn collective behaviors observed from surrounding through various mechanisms such as imitation, enhancement and conditioning. This mechanism is expected to accelerate the learning rate of an individual because it prevents the incurring of excessive computational costs contributed by individual trial and error. In the context of NSTLBO-MLPs, social learning was implemented in modified teacher phase by assuming each n-th learner is able to observe and imitate the group of other $(n-1)$ learners in classroom with lower Pareto ranks and/or higher CD values in enhancing its knowledge level. Let $m \in [1, .., n]$ be the index of any NSTLBO-MLPs learner with better Pareto rank or CD than that of n-th learner, the corresponding mean position represented using $\tilde{X}_n^{mean}$ can be derived as follows:

$$\tilde{X}_n^{mean} = \frac{\sum_{m=1}^{n} X_m}{n} \tag{11}$$

From Eq. (11),the mean position $\tilde{X}_n^{mean}$ assigned to each n-th learner is unique because different groups of learners are considered in the formulation process. Notably, Eq. (11) is not applicable for the best learner with index value of $n = 1$ because none of the population members has lower Pareto rank and/or larger CD than that of it. Different approach was proposed to derive a unique mean position $\tilde{X}_{best}^{mean}$ for the best learner by leveraging the useful information of all $|F_1|$ non-dominated solutions obtained from the first level of Pareto front F_1. Define $r_a \in [0, 1]$ as a randomly generated number assigned to each a-th non-dominated solution X_a in F_1 to indicate its weightage contribution in deriving the mean position $\tilde{X}_{best}^{mean}$ of best learner as shown in Eq. (12). Different $\tilde{X}_{best}^{mean}$ is obtained in each generation of NSTLBO-MLPs in guiding the best learner in order to preserve the population diversity.

$$\tilde{X}_{best}^{mean} = \frac{\sum_{a=1}^{|F_1|} r_a X_a}{\sum_{a=1}^{|F_1|} r_a} \tag{12}$$

Referring to the closest teacher and unique mean position obtained by each n-th NSTLBO-MLPs learner, a modified learner phase is designed to calculate its new solution as follows:

$$X_n^{new} = \begin{cases} X_n + r_3 \left(X_n^{teacher} - T_{f1} X_n \right) + r_4 \left(\tilde{X}_n^{mean} - T_{f2} X_n \right), & \text{if } n = 2, ..., N \\ X_n + r_3 \left(X_n^{teacher} - T_{f1} X_n \right) + r_4 \left(\tilde{X}_{best}^{mean} - T_{f2} X_n \right), & \text{if } n = 1 \end{cases} \tag{13}$$

where $r_3, r_4 \in [0, 1]$ are two uniformly distributed random numbers; $T_{f1}, T_{f2} \in [1, 2]$ are two uniformly distributed teaching factors used to indicate different levels of learning tendency from the teacher and mainstream knowledge, respectively, aiming to achieve more realistic emulation of classroom teaching and learning process [49]. Unlike conventional TLBO, the modified teacher phase of NSTLBO-MLPs allows each learner to enhance its knowledge level by interacting with the nearest teacher in classroom while imitating the collective behaviors of other group of promising learners simultaneously as shown in Fig. 9. All knowledge from teacher and other groups of promising learners are assumed to be imparted to each NSTLBO-MLPs learners successfully if $T_{f1} = T_{f2} = 2$. In contrary, the learner is considered fail to learn any useful knowledge when T_{f1} and T_{f2} are set as 1 [49].

3.3.4. *Modified learner phase of NSTLBO-MLPs*

Exploration search of the conventional TLBO was emphasized via a repulsion mechanism incorporated into learner phase of Eq. (10) that aims to discourage the convergence of each n-th learner towards a randomly selected peer learner with worse fitness. Nevertheless, it is a non-trivial to trigger this

Algorithm 3: $X_n^{teacher}$ = **Teacher_Selection** (F_1, X_n, n, X^U, X^L)

1: Discard X_n from F_1 if X_n is one of the non-dominated solution stored in F_1;
2: Calculate total number of eligible candidate teachers stored in F_1 as $|F_1|$;
3: **for** $a = 1$ to $|F_1|$ **do**
4: Determine the $E_{n,a}$ value between each n-th learner and a-th candidate teacher with Eq. (7);
5: **end for**
6: Identify the a-th candidate teacher with smallest $E_{n,a}$ as the $X_n^{teacher}$ of n-th learner;

Fig. 8 – Pseudo-code used to assign a unique teacher for each NSTLBO-MLPs learner in guiding the search process during the modified teacher phase.

Algorithm 4: X_n^{new} = **Modified_Teacher_Phase**(F_1, X_n, n, X^U, X^L)

1: $X_n^{teacher}$ = **Teacher_Selection** (F_1, X_n, n, X^U, X^L); /*Algorithm 3*/
2: **if** n is not equal to 1 **then**
3: Calculate $\tilde{X}_n^{mean}$ of each n-th learner using Eq. (11);
4: **else** /*only for the best learner*/
5: Calculate $\tilde{X}_{best}^{mean}$ ofbest learner using Eq. (12);
6: **end**
7: Randomly generate $T_{f1}, T_{f2} \in [1,2]$;
8: Determine the X_n^{new} of n-th learner using Eq. (13);

Fig. 9 – Pseudo-code used to summarize the modified teacher phase of NSTLBO-MLPs.

repulsion mechanism in the MOPs which consists of multiple and/or conflicting objective functions, because the probability of identifying peer learner that can be completely dominated by a given n-th learner is reduced significantly. As a search process progresses to the later stages of optimization, no drastic changes of population diversity is observed, because majority of learners stagnate at the similar regions of search space and they tend to become indistinguishable from each other. This scenario also contributes to the reduced likelihood of triggering Eq. (7) to provide additional momentum for TLBO learners in escaping from the local Pareto front of complex MOPs. In order to overcome these drawbacks, two strategies aiming to enhance exploration strength of NSTLBO-MLPs were proposed in modified learner phase.

Motivated by real-world teaching and learning paradigm, it is assumed that different types of learners with their preferred learning methods exist in the classroom. For instance, certain learners prefer to obtain new knowledge by interacting with their peers, while some of them are self-directed learners that take initiative to achieve knowledge enhancement through a crucial skill known as independent learning that becomes increasingly important in modern educational climate. In order to enhance the robustness of NSLTBO-MLPs learning framework, a stochastic-based mutation scheme was proposed in modified learner phase to facilitate independent learning for all self-directed learners with a mutation probability of $P^{MUT} = 1/D$. After completing the modified teacher phase, an independent learning was performed on the randomly selected dimension of each n-th self-directed learner (i.e.,X_{n,d_r}) via random perturbation, where $d_r \in [1, D]$. Let X_{n,d_r}^{new} be the perturbed component of n-th self-directed learner, then:

$$X_{n,d_r}^{new} = X_{n,d_r} + r_5 \left(X_{d_r}^U - X_{d_r}^L \right) \tag{14}$$

where $r_5 \in [-1, 1]$ is a uniformly distributed random number; X_{n,d_r}^{new} refers to the new solution obtained by n-th self-directed learner in d_r-th dimension; $X_{d_r}^U$ and $X_{d_r}^L$ represent the upper and lower boundary values in every d_r-th dimension, respectively. Fig. 10 summarizes the mechanism of independent learning adopted by each n-th self-directed learner.

Meanwhile, an adaptive peer learning mechanism was designed for the remaining learners that are keen to achieve knowledge enhancement through peer interactions. For conventional TLBO, each learner can only interact with one randomly selected peer to update all of its dimensional components simultaneously as shown in Eqs. (6) and (7). These formulations, however, might not be able to describe the actual teaching and learning scenario in classroom accurately, because a peer learning process is generally expected to be effective if every learner is allowed to interact with more than one peer. Furthermore, different learners might be more knowledgeable in certain courses (i.e., dimensional component), hence only those weaker courses have higher urgency to be improved further through peer interaction. Motivated by these observations, a more realistic version of peer learning strategy was proposed in the modified learner phase for improving the performance of NSTLBO-MLPs further.

Algorithm 5: X_n^{new} = **Independent_Learning** (X_n , D, X^U , X^L)

1: Randomly generate $d_r \in [1, D]$ for each n-th self-directed learner;
2: Identify the d_r -th dimensional component of X_n , X^U , and X^L ;
3: Calculate the perturbed solution of n-th self-directed learners X_{n,d_r}^{new} with Eq. (14);

Fig. 10 – Pseudo-code of independent learning for self-directed learner in modified learner phase of NSTLBO-MLPs.

After completing the modified teacher phase as explained in previous subsection, all NSTLBO-MLPs learners were rearranged according to their respective Pareto rank and CD values, where the n-th learner with smaller $Rank_n$ and/or larger values Δ_n is assigned with smaller index value of n and vice versa. Define $P_n^{PL} \in [0, 1]$ as the peer learning probability of each n-th learner, then:

$$P_n^{PL} = \frac{n}{N} \tag{15}$$

Based on the peer learning probability P_n^{PL} obtained, every n-th NSTLBO-MLPs learner can the generate the new solution X_n^{new} by using the procedures described as follows. For each d-th dimension of X_n^{new} (i.e.,$X_{n,d}^{new}$), a random number $r_6 \in [0, 1]$ is first generated using uniform distribution and then compared with the peer learning probability P_n^{PL} of n-th learner. If r_6 is smaller than P_n^{PL}, three peer learners denoted as X_j, X_k and X_l are randomly selected from the NSTLBO-MLPs population to produce a new value of $X_{n,d}^{new}$ as shown in Eq. (16) where $n \neq j \neq k \neq l$. Otherwise, the n-th learner can retain is original $X_{n,d}$ value in $X_{n,d}^{new}$. Define $\phi_n \in [0.5, 1]$ as the peer learning factor of n-th learner that is randomly generated from uniform distribution. The adaptive peer learning strategy of NSTLBO-MLPs is then formulated as:

$$X_{n,d}^{new} = \begin{cases} X_{j,d} + \phi_n (X_{k,d} - X_{l,d}), & \text{if } r_6 < P_n^{PL} \\ X_{i,d}, & \text{otherwise} \end{cases} \tag{16}$$

From Eqs. (15) and (16), the n-th learner with inferior Pareto rank and crowding distance values is assigned with higher P_n^{PL}. Hence, it has higher tendency to interact with its peers in updating most of its dimensional components of X_n^{new} as compared with that with lower P_n^{PL} due to the better Pareto rank and crowding distance values. In contrast to TLBO, the adaptive peer learning strategy of NSTLBO-MLPs not only allows each learner to interact with multiple peers in enhancing its knowledge, but it can also adaptively determine the tendency of learner to update its dimensional components via peer interaction by referring to its Pareto rank and CD values. To this end, the pseudocode used to describe modified learner phase of NSTLBO-MLPs is presented in Fig. 11.

3.3.5. *Fuzzy decision maker*

If a given MOP is solved using posterior method, the optimization output obtained is represented as the first level of Pareto front F_1. While all solution members of F_1 are non-dominated with each other, the most desirable Pareto optimal solution needs to be determined by process planner to achieve the goals of MOPs by ensuring the relative significance of objective functions provided. A decision making process known as fuzzy decision maker was incorporated into NSTLBO-MLPs to address the aforementioned issue.

Assume that a given MOP with M objective functions consist of a set of utopia point in objective space represented using $\Psi^U = [\Psi_1^U, .., \Psi_m^U, ..., \Psi_M^U]$, where each utopia point indicates the best possible value of the$m$-th objective, where m = 1,..,M. In contrary, the worst possible values for all M objectives are represented in objective space using a set of pseudo nadir point of $\Psi^{SN} = [\Psi_1^{SN}, .., \Psi_m^{SN}, ..., \Psi_M^{SN}]$. Define $\Psi_m(X_a)$ as the objective function value obtained by every a-th solution stored in Pareto front F_1 in solving the m-th objective, while the corresponding membership value is represented using μ_a^m, where $a = 1, .., |F_1|$ and $m = 1, .., M$. The values of μ_a^m used to address the minimization MOPs can be determined using a fuzzification process described as below:

$$\mu_a^m = \begin{cases} 1, & \Psi_m(X_a) < \Psi_m^U \\ \dfrac{\Psi_m^{SN} - \Psi_m(X_a)}{\Psi_m^{SN} - \Psi_m^U}, & \Psi_m^U \leq \Psi_m(X_a) \leq \Psi_m^{SN} \\ 0, & \Psi_m(X_a) > \Psi_m^{SN} \end{cases} \tag{17}$$

Apart from the membership values, the relative weightage of all objective functions were also considered as crucial information required by process planner in selecting the most desirable Pareto optimal solution. Denote w_m as the weightage value that reflects the degree of importance for each m-th objective, while μ_a be the total degree of optimality for each a-th solution in F_1 after considering all M objective functions. Therefore,

$$\mu_a = \sum_{m=1}^{M} w_m \mu_a^m \tag{18}$$

The a-th non-dominated solution that obtains larger μ_a value was considered to produce better optimization of a given MOP and vice versa. Define $X^{preferred}$ as the most desirable Pareto optimal solution corresponds to the degree of importance defined for all objective functions. Then, the a-th solution of F_1 with the largest value of μ_a was determined as $X^{preferred}$ according to Fig. 12.

3.3.6. *The complete NSTLBO-MLPs*

The overall algorithmic framework of NSTLBO-MLPs are summarized in Fig. 13, where γ represents a counter used to record the number of fitness evaluation performed so far and Γ defines the termination condition of NSTLBO-MLPs known as maximum fitness evaluation numbers. A popula-

Algorithm 6: X_n^{new} = **Modified_Learner_Phase** (X_n, D,X^U, X^L, P_n^{PL} , P^{MUT})

Randomly generate $rand \in [0,1]$;
if $rand \le P^{MUT}$ **then** /*Independent learning for self-directed learners*/
  X_n^{new} = **Independent_Learning** (X_n , D, X^U , X^L);
else /*Perform adaptive peer-learning for the remaining learners*/
  for $d = 1$ to D **then**
    Calculate $X_{i,d}^{new}$ using Eq. (16);
  end for
end if

Fig. 11 – Pseudo-code of modified learner phase in NSTLBO-MLPs.

Algorithm 7: $X^{preferred}$ = **Fuzzy_Decision_Maker** (F_1, M, w_m)

Identify the total number of non-dominated solutions stored in the first level of Pareto front F_1 as $|F_1|$;
for $a = 1$ to $|F_1|$ **do**
  for $m = 1$ to M **do**
    Evaluate the fitness value of X_a in each m-th objective function;
  end for
end for
Identify $\Psi^U = [\Psi_1^U, .., \Psi_m^U, ..., \Psi_M^U]$ and $\Psi^{SN} = [\Psi_1^{SN}, .., \Psi_m^{SN}, ..., \Psi_M^{SN}]$ in the objective space;
for $a = 1$ to $|F_1|$ **do**
  for $m = 1$ to M **do**
    Calculate the value of μ_a^m for X_a in each m-th objective function with Eq. (14);
  end for
  Determine the value of μ_a for X_a with Eq. (15);
end for
Select the a-th non-dominated solution X_a with the largest value of μ_a to be $X^{preferred}$;

Fig. 12 – Pseudo-code of fuzzy decision maker incorporated into NSTLBO-MLPs.

tion **P** that consists of N learners was first initialized and their fitness value for all M objectives were then evaluated. This was followed by the computation of Pareto rank, Pareto front layer and CD values of all NSTLBO-MLPs learners. Based on these information, the crowding-comparison operator was then applied to sort the population members in **P** from the best to worst. The learner X_n with smaller $Rank_n$ and/or larger values Δ_n was assigned with smaller index value of n and vice versa.

While the termination condition of NSTLBO-MLPs was not satisfied, the new solution of every n-th learner (i.e.,X_n^{new}) was produced with the search operators introduced in both of the modified teacher and learner phases. These N offspring solutions were stored in an offspring population $\mathbf{P}^{off}$ and then merged with the main population **P** to construct a combined population of $\mathbf{P}^{comb} = \mathbf{P} \cup \mathbf{P}^{off}$ that has a population size of $2N$. All solution members of $\mathbf{P}^{comb}$ were then sorted from best to worst using the CD operator. The best N population members were truncated from $\mathbf{P}^{comb}$ using a $Trunc(\cdot,\cdot)$ operator to form a new main population of NSTLBO-MLPs in the next learning phase. The aforementioned search procedures were repeated until the satisfaction of termination condition where $\gamma > \Gamma$. Finally, the most preferred Pareto optimal solution $X^{preferred}$ was determined from the first level of Pareto front F_1 using fuzzy decision maker based on the degree of significance of all objective functions specified in achieving the desired goal of MOP.

3.3.7. *Performance metrics*

Two metrics were adopted to assess optimization performances demonstrated by the proposed algorithm and six well-established metaheuristic search algorithms. The quality between two Pareto fronts can be differentiated by calculating the number of solution members denominated by each other. Assume that F_1^A and F_1^B are two Pareto fronts obtained from compared algorithms, the coverage operator is then defined as:

$$Cov\left(F_1^A, F_1^B\right) = \frac{\left|\left\{b \in F_1^B; \exists a \in F_1^A : a \prec= b\right\}\right|}{\left|F_1^B\right|} \tag{19}$$

As shown in Eq. (19), if all solution members of Pareto front F_1^A can dominate or at least perform equally with those of F_1^B, then $Cov\left(F_1^A, F_1^B\right) = 1$. Otherwise, the output of $Cov\left(F_1^A, F_1^B\right) = 0$ is obtained, implying that none of the solution members of F_1^B are dominated by those of F_1^A. Furthermore, it is noteworthy that $Cov\left(F_1^A, F_1^B\right)$ is not necessary equal to $1 - Cov\left(F_1^B, F_1^A\right)$, hence these two results need to be presented together in performance analysis.

Algorithm 8: NSTLBO-MLPs

Reset the counter used to capture the number of fitness evaluation performed so far as $\gamma = 0$;
for $n = 1$ to N **do**
  Initialize the position vector of each n-th learner randomly;
  Evaluate the fitness values of each n-th learner for all M objective functions;
  $\gamma \leftarrow \gamma + M$;
end for
Define **P** as a current population to store all NSTLBO-MLPs learners;
[**F, R**]= **Fast_Non_Dominated_Sorting** (**P**); */*Algorithm 1*/*
Δ = **Crowding_Distance_Calculation** (**F**); */*Algorithm 2*/*
Apply crowding-comparison operator to sort on all members of **P**;
while $\gamma \leq \Gamma$ **do**
  */*Execute modified teacher phase using Algorithm 4*/*
  for $n = 1$ to N **do**
    X_n^{new} = **Modified_Teacher_Phase**(F_1, X_n, n, X^U, X^L);
    Evaluate the fitness values of each n-th leaner for all M objective functions;
    $\gamma \leftarrow \gamma + M$;
  end for
  Store all new offspring solutions into $\mathbf{P}^{off}$;
  $\mathbf{P}^{comb} = \mathbf{P} \cup \mathbf{P}^{off}$;
  [**F, R**]= **Fast_Non_Dominated_Sorting**($\mathbf{P}^{comb}$); */*Algorithm 1*/*
  Δ = **Crowding_Distance_Calculation** (**F**); */*Algorithm 2*/*
  Apply crowding-comparison operator to sort all members of $\mathbf{P}^{comb}$;
  $\mathbf{P} \leftarrow Trunc\left(\mathbf{P}^{off}, N\right)$; */*Truncate the N best members*/*
  */*Execute modified learner phase using Algorithm 6*/*
  for $n = 1$ to N **do**
    X_n^{new} = **Modified_Learner_Phase** (X_n, D,X^U, X^L, P_n^{PL} , P^{MUT});
    Evaluate the fitness values of each n-th leanerfor all M objective functions;
    $\gamma \leftarrow \gamma + M$;
  end for
  Store all new offspring solutions into $\mathbf{P}^{off}$;
  $\mathbf{P}^{comb} = \mathbf{P} \cup \mathbf{P}^{off}$;
  [**F, R**]= **Fast_Non_Dominated_Sorting**($\mathbf{P}^{comb}$); */*Algorithm 1*/*
  Δ = **Crowding_Distance_Calculation** (**F**); */*Algorithm 2*/*
Apply crowding-comparison operator to sort all members of $\mathbf{P}^{comb}$;
  $\mathbf{P} \leftarrow Trunc\left(\mathbf{P}^{off}, N\right)$; */*Truncate the N best members*/*
end while
Identify the first level of Pareto front as F_1;
$X^{preferred}$ = **Fuzzy_Decision_Maker** (F_1, M, w_m); */*Algorithm 7*/*

Fig. 13 – Pseudo-code of complete NSTLBO-MLPs.

The second metric introduced is known as spacing metric that aims to quantify the solution diversity of Pareto front produced by each compared algorithm. Denote $|F_1|$ as the number of non-dominated solutions stored in the Pareto front F_1 after optimizing M objective functions, while d_a represents the minimum Euclidean distance between a-th and b-th solution members of F_1 in the objective space for the m-th objective function. Then,

$$d_a = \min_{a,a \neq b} \sum_{m=1}^{M} \left| \Psi_m(X_a) - \Psi_m(X_b) \right|, \; a, b = 1, \ldots, |F_1| \tag{20}$$

Let $\bar{d}$ be the average value of d_a for all non-dominated solutions of F_1 and it is calculated as:

$$\bar{d} = \frac{\sum_{a=1}^{|F_1|} d_a}{|F_1|} \tag{21}$$

Finally, the distance variances of neighboring non-dominated solutions in F_1 are quantified through a spacing metric S defined as:

$$S = \sqrt{\frac{1}{|F_1| - 1} \sum_{a=1}^{|F_1|} \left(\bar{d} - d_a\right)^2} \tag{22}$$

As shown in Eq. (22), Pareto optimal solution set obtained are considered to be more uniformly distributed if S has a smaller value. The ideal value of S is equal to zero because this implies all solution members of F_1 are equidistant from one another.

4. Predicted results and experimental validation

The proposed algorithm was applied into regression models (Eqs 1–3) to predict the maximum lap shear load, maximum hardness and minimum wear. Suppose that w_1,

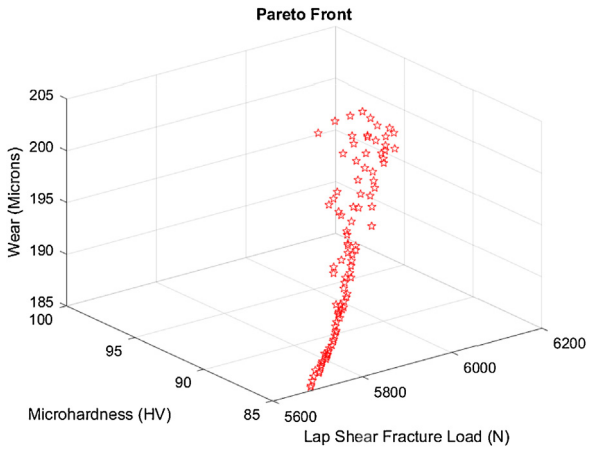

Fig. 14 – The Pareto front ofNSTLBO-MLP – Prediction of Optimum SFSSW Parameters.

w_2 and w_3 represent the three weighting terms indicating the relative importance levels of maximization of lap shear load, maximization of microhardness, and minimization of wear respectively, where $w_1 + w_2 + w_3 = 1$. Given the relative importance levels of $w_1 = w_2 = w_3 = 1/3$, the optimum welding parameters of $D = 2.8$ mm, N =1387 rpm and $F = 17$ mm/minute were obtained from NSTLBO-MLPs with the predicted wear, lap shear fracture load and microhardness values of 197 microns, 6134 N and 94.6 HV, respectively. Fig. 14 shows the Pareto front of proposed NSTLBO-MLP with a population of N = 100. The predicated optimum welding parameters from NSTLBO-MLPs were further used to conduct validation experiments. The same procedure as discussed in sections 2.3-2.4 was followed in order to determine the respective response variables.

Table 6 presents the predicted values from NSTLBO-MLPs and actual values measured from experiments for the same optimal condition. Based on the validation results reported, the minimal errors of 0.179%, 0.317% and 0.507% were observed between the actual and predicted results of lap shear load, microhardness and wear, respectively. Noting the negligible errors, it can be concluded that the proposed NSTLBO-MLPs is applicable to solve the real-world welding optimization problem with promising results. Moreover, the proposed method and predicted SFSSW process parameters can be adopted by industries for welding AA6061-T6 components in order to have good quality weld joints.

In order to ensure the effectiveness of the newly developed NSTLBO-MLPs algorithm, the further simulation studies were conducted with six well-established metaheuristic search algorithms. The overall quality of Pareto front of NSTLBO-MLP is compared with the Pareto fronts of six other metaheuristic search algorithms and reported in Section 4.1.

4.1. *Performance analysis of NSTLBO-MLPs and comparison of simulation results*

The optimization performances of NSTLBO-MLPs in addressing multi-objective welding problems were evaluated with six existing metaheuristic search optimization algorithms known as: MOPSO (Multi-Objective Particle Swarm Optimization) [54], NSGA-II (Non-dominated Sorting Genetic Algorithm II) [55], MOGWO (Multi-Objective Grey Wolf Optimizer) [56], MOTLBO (Multi-Objective Teaching-Learning Based Optimization) [49], MO-ITLBO (Multi-Objective Improved Teaching-Learning Based Optimization) [57] and NSTLBO (Non-dominated Sorting Teaching-Learning Based Optimization [51]. These algorithms were reported to have competitive search performances in the past literature. The parameters of all compare-optimizers were set as per stated in their original literatures as summarized in Table 7.

Both concepts of FNDS and CD were leveraged by NSGA-II, MOTLBO, NSTLBO and NSTLBO-MLPs in ranking the quality of non-dominated solutions obtained during the search process. Meanwhile, the MOPSO, MOGWO and MO-ITLBO were incorporated with an archive to keep the good quality solutions. Two parameters used to construct the archive of MPSO and MOGWO were set as $\alpha = 0.1$ and $nGrid = 10$.The inertia weight ω of MPSO was a time-varying parameter that can be linearly reduced from an upper limit of 0.9 to a lower limit of 0.4, whereas both acceleration coefficients was the fixed parameters of $c_1 = c_2 = 2.05$. The same mutation probability of $P_{mut} = 1/D$ was set for MOPSO, NSGA-II and NSTLBO-MLPs incorporated with a stochastic-based mutation scheme [54,55]. Furthermore, the crossover probability of NSGA-II was assigned with $P_{cr} = 0.9$. For MO-ITLBO, the parameter setting of $\varepsilon = 0.007$ was used to manage the external achieve, while a sub-populations size of $nGroup = 4$ was set during the teacher phase to achieve better balancing of exploration and exploitation searches [57]. In contrast to NSTLBO that only has two discrete values of teaching factor with $T_f \in \{1, 2\}$, the teacher factors assigned to the remaining TLBO variants of MOTLBO, MO-ITLBO and NSTLBO-MLPs were uniformly distributed between 1 and 2, aiming to indicate different tendency of learners to learn from their teacher and the mainstream knowledge.

The population sizes of $N = 50$, 75 and 100 were set for all compare-optimizers in order to study the effect of N on their optimization performances. The archive sizes of MOPSO, MOGWO and MO-ITLBO were set to be same as to their population size, where, $|A| = N$. The same maximum fitness evaluation number of $\Gamma = 50,000$ was defined to be termination conditions for all selected optimizers to ensure fairness in comparisons. All seven compare-optimizers were coded using Matlab 2019a software on a personal computer with Intel ® Core i7-7500 CPU @ 2.70 GHz. The average results were obtained by simulating each selected optimizer for 20 times. The mean and standard deviation (*SD*) values of coverage metrics obtained in the performance evaluation between NSTLBO-MLPs and six other optimizers are summarized in Table 8.

As reported in Table 8, the proposed NSTLBO-MLPs has demonstrated outstanding optimization performance among all compared optimizers in all population sizes because it can produce the Pareto fronts that consist of the largest numbers of non-dominated solutions for $N = 50$, 75 and 100. For instance, it is reported that 17.9% of solution members in the MOPSO's Pareto front are inferior to those in NSTLBO-MLPs for $N = 100$, while only 3.3% of the members of Pareto

Table 7 – Parameter settings of all compare-optimizers.

Optimizers	Parameter settings
MOPSO	$N, \lvert A\rvert \in \{50, 75, 100\}, \omega \in 0.9 \rightarrow 0.4, c_1 = c_2 = 2.05, P_{mut} = 1/D, \alpha = 0.1, nGrid = 10$
NSGA-II	$N \in \{50, 75, 100\}, P_{cr} = 0.9, P_{mut} = 1/D$
MOGWO	$N, \lvert A\rvert \in \{50, 75, 100\}, \alpha = 0.1, nGrid = 10$
MOTLBO	$N \in \{50, 75, 100\}, T_f \in [1, 2]$
MO-ITLBO	$N, \lvert A\rvert \in \{50, 75, 100\}, nGroup = 4, T_f \in [1, 2], \varepsilon = 0.007$
NSTLBO	$N \in \{50, 75, 100\}, T_f \in [1, 2]$
NSTLBO-MLPs	$N \in \{50, 75, 100\}, P_{mut} = 1/D, T_{f1}, T_{f2} \in [1, 2]$

Table 8 – Performance evaluation - coverage metrics of optimizers.

Compared sets	$N = 50$		$N = 75$		$N = 100$	
	Mean	*SD*	Mean	*SD*	Mean	*SD*
$Cov(\mathbf{R}_P, \mathbf{S}_P)$	0.120	0.039	0.160	0.031	0.179	0.033
$Cov(\mathbf{S}_P, \mathbf{R}_P)$	0.030	0.019	0.041	0.022	0.033	0.018
$Cov(\mathbf{R}_P, \mathbf{T}_P)$	0.128	0.078	0.095	0.028	0.121	0.032
$Cov(\mathbf{T}_P, \mathbf{R}_P)$	0.038	0.030	0.057	0.018	0.056	0.021
$Cov(\mathbf{R}_P, \mathbf{U}_P)$	0.144	0.044	0.132	0.031	0.159	0.020
$Cov(\mathbf{U}_P, \mathbf{R}_P)$	0.030	0.017	0.047	0.028	0.026	0.022
$Cov(\mathbf{R}_P, \mathbf{V}_P)$	0.130	0.045	0.173	0.031	0.144	0.048
$Cov(\mathbf{V}_P, \mathbf{R}_P)$	0.038	0.033	0.039	0.025	0.030	0.024
$Cov(\mathbf{R}_P, \mathbf{W}_P)$	0.126	0.049	0.146	0.047	0.168	0.077
$Cov(\mathbf{W}_P, \mathbf{R}_P)$	0.026	0.021	0.039	0.021	0.031	0.019
$Cov(\mathbf{R}_P, \mathbf{X}_P)$	0.100	0.013	0.211	0.041	0.198	0.038
$Cov(\mathbf{X}_P, \mathbf{R}_P)$	0.054	0.013	0.053	0.023	0.036	0.016

Remark: The sets of $\mathbf{R}_P$, $\mathbf{S}_P$, $\mathbf{T}_P$, $\mathbf{U}_P$, $\mathbf{V}_P$, $\mathbf{W}_p$ and $\mathbf{X}_p$ are used to represent the Pareto fronts obtained by NSTLBO-MLPs, MOPSO, NSGA-II, MOGWO, MOTLBO, MO-ITLBO and NSTLBO in optimizing the multi-objective welding problem.

front produced by NSTLBO-MLPs are dominated by those of MOPSO. For $N = 50$, a total of 12.8% and 14.4% of solution members in the Pareto fronts produced by NSGA-II and MOGWO, respectively, are outperformed by those of NSTLBO-MLPs. In contrary, the numbers of inferior solutions in Pareto front of NSTLBO-MLPs are at least three times fewer than those of NSGA-II and MOGWO for $N = 50$. Among all TLBO variants selected for performance evaluation, MOTLBO is reported to have the worst performance for $N = 50$, because it has the highest number of solution members in Pareto front (i.e., 13.0%) that are dominated by those of NSTLBO-MLPs, whereas only 3.8% of Pareto front members obtained by NSTLBO-MLPs are inferior to MOTLBO. The worst performing algorithm for both population sizes of $N = 75$ and 100 is NSTLBO because a total of 21.1% and 19.8% of solution members in Pareto fronts, respectively, are outperformed by the NSTLBO-MLPs. In contrary, there are less than 6% of Pareto optimal solutions obtained by NSTLBO-MLP are performing worse than those of NSTLBO in all population sizes. The simulation results in Table 8 imply that the approximated Pareto fronts generated by the proposed NSTLBO-MLPs in solving the multi-objective SFSSW problem are much closer to the true Pareto front than other optimizers. The excellent quality of Pareto fronts produced by NSTLBO-MLPs prove that the proposed modifications are indeed able to provide more accurate modelling of teaching and learning paradigm in classroom. To this end, better balancing of exploration and exploitation strengths can be achieved during the search process of NSTLBO-MLPs learners and this leads to the improvement of its search performance.

The mean and standard deviation (*SD*) values of spacing metric in the Pareto fronts generated by all seven compare-optimizers for all population sizes of $N = 50$, 75 and 100 are summarized in Table 9. Notably, NSTLBO-MLPs is revealed as the best performing algorithm due to the lowest mean spacing values obtained in all population sizes, implying that the solutions members of Pareto fronts obtained are the most diversified and evenly distributed as compared to those of six other peer algorithms. Drastic observations are demonstrated by the NSTLBO and NSGA-II that produce the second lowest and largest mean spacing values, respectively. Particularly, the Pareto front of NSGA-II has the poorest distributions as indicated by its largest mean spacing values in all population size although it has less solution members dominated by those of NSTLBO-MLPs. The unsatisfactory of solution diversity in NSGA-II's Pareto fronts generated suggests the presence of duplicated Pareto optimal solutions, hence leading to good solution accuracy in terms of coverage metric and poor solution diversity in terms of spacing values. In contrary, NSTLBO tends to produce higher number of inferior Pareto solution members in spite of having better distribution of Pareto fronts (i.e., the second lowest mean *S* values). This implies that although all Pareto front members of NSTLBO are uniformly distributed, majority of these solutions are trapped in the local optimal regions due to the rapid diversity loss of populations. As compared with NSTLBO and NSGA-II, the proposed NSTLBO-MLPs is able to achieve better balancing in producing good quality as well as well distributed solution members in the Pareto fronts. The teacher selection scheme and social learning concept

Table 9 – Performance evaluation - spacing metric of all optimizers.

Algorithm	N = 50		N = 75		N = 100	
	Mean	SD	Mean	SD	Mean	SD
MOPSO	4.443	0.345	6.5951	0.3655	8.826	0.355
NSGA-II	4.616	0.504	7.8765	1.5725	10.166	1.398
MOGWO	4.364	0.407	6.4941	0.2270	8.630	0.279
MOTLBO	4.449	0.280	7.1401	0.5902	8.852	0.339
MO-ITLBO	4.505	0.469	6.6347	0.2711	8.514	0.306
NSTLBO	4.199	0.154	6.4716	0.2666	8.558	0.324
NSTLBO-MLPs	3.842	0.188	5.9451	0.3297	7.795	0.199

incorporated into the modified teacher phase enables each NSTLBO-MLPs learners to search different regions of search space, hence ensuring the uniform distribution of Pareto front members. Meanwhile, the independent learning and adaptive peer learning mechanism introduced into the modified teacher phases are useful in providing additional momentum to the population members to break through the inferior solution areas in search space and continue to approach towards the true Pareto fronts.

The Pareto-fronts generated by all compare-optimizers in solving multi-objective SFSSW problem for $N = 100$ are illustrated in Fig. 15. The qualitative performance analyses reported in Fig. 15 are generally consistent with those of quantitative results in Tables 8 and 9. It is notable that the Pareto front of NSGA-II is significantly different with those of the remaining algorithms because most of NSGA-II's solution members fail to converge towards the true Pareto front due to rapid loss of solution diversity. The inferior optimization performance of NSGA-II in searching for the best parameters of welding process is also demonstrated in the previous quantitative analyses. Although the solution members of Pareto front produced by MOGWO and MOPSO are closer towards the true Pareto front, these two optimizers produced less uniformly distributed solutions at the top region of Pareto front as compared with those of NSTLBO-MLPs, revealing the weakness of former two algorithms in exploring the certain parts of objective space. Similar behaviors are demonstrated by the MOTLBO and MO-ITLBO because of the existence of significant discontinuities regions observed at the bottom parts of their Pareto fronts. The NSTLBO and NSTLBO-MLPs produce equally good Pareto fronts because these two algorithms share certain similarity levels in term of search mechanisms. Nevertheless, quantitative results in both Tables 9 and 10 show that the proposed NSTLBO-MLPs demonstrated more promising optimization performance because it can achieve the best tradeoff of accuracy and diversity of solutions by referring to the Pareto fronts generated. Unlike NSTLBO, the social learning mechanism incorporated to obtain the unique mean position for each NSTLBO-MLPs learner enables it to outreach more unvisited regions of search space by exploring around those solutions better than it.

Furthermore, both of the independent learning and adaptive peer learning mechanism of NSTLBO-MLPs also enables each learner to perform searching with more balanced exploration and exploitation strengths, hence are effective in maintaining the diversity of solution members in Pareto front.

5. Discussions on weld sample prepared at optimal condition

To analyse the improvement in SFSSW sample prepared at optimal condition, the respective microstructure of weld cross-section, fracture surfaces, and wear surface were examined using field emission scanning electron microscope (FESEM model: SIGMA - Carl Zeiss). The cross section of the weld samples was firstly prepared and etched with Keller's reagent to study the microstructure of the stir zone (SZ). The FESEM micrograph of SZ of Al_2O_3 added SFSSW sample prepared with the optimal condition ($D = 2.8$ mm, $N = 1387$ rpm and $F = 17$ mm/minute) is shown in Fig. 16.

Fig. 16(a) shows a homogeneous distribution of Al_2O_3 nanoparticles in SZ of AA6061-T6/Al_2O_3 weld joint, which was caused by dynamic recrystallization. The dynamic recrystallization is due to the frictional heat that caused a severe plastic deformation during the SFSSW process and the addition of Al_2O_3 nanoparticles as well. The Al_2O_3 nanoparticles are perfectly visible and excellent coherency with the aluminium matrix in the grain boundaries is seen as shown Fig. 16(b). Most of the Al_2O_3 particles are seen placed in the grain boundaries which could lead to grain growth prevention [58]. It is obvious that the placement of reinforced particles at the grain boundaries and the uniform dispersion of the particles are the reason for the improvement in mechanical properties of SFSSW joint.

In other hand, Fig. 17 shows the FESEM micrograph of the weld sample prepared with condition ($D = 3$ mm, $N = 1800$ rpm and $F = 10$ mm/minute). It consists of Al_2O_3 nanoparticles agglomeration that resulted the lower mechanical properties. The agglomeration of Al_2O_3 nanoparticles increased the interface area with aluminium matrix and showed the poor bonding between Al_2O_3 and aluminium. It is clearly understood that the presence of nanoparticle agglomeration in SZ due to non-homogeneous distribution affects the weld strength.

Welding defects such as cavities, tunnels, hook and wormhole may occur due to improper process parameters or technological conditions detrimental to the mechanical performance of the joint [59]. In the present study, the major defects such as wormhole defect, insufficient fill and cavity formation were observed during the trial experiments as listed in Table 2. But, the sample prepared at optimal condition does not show any of such major defects. Hook defect and keyhole (shape same as tool pin) are generally formed at the weld

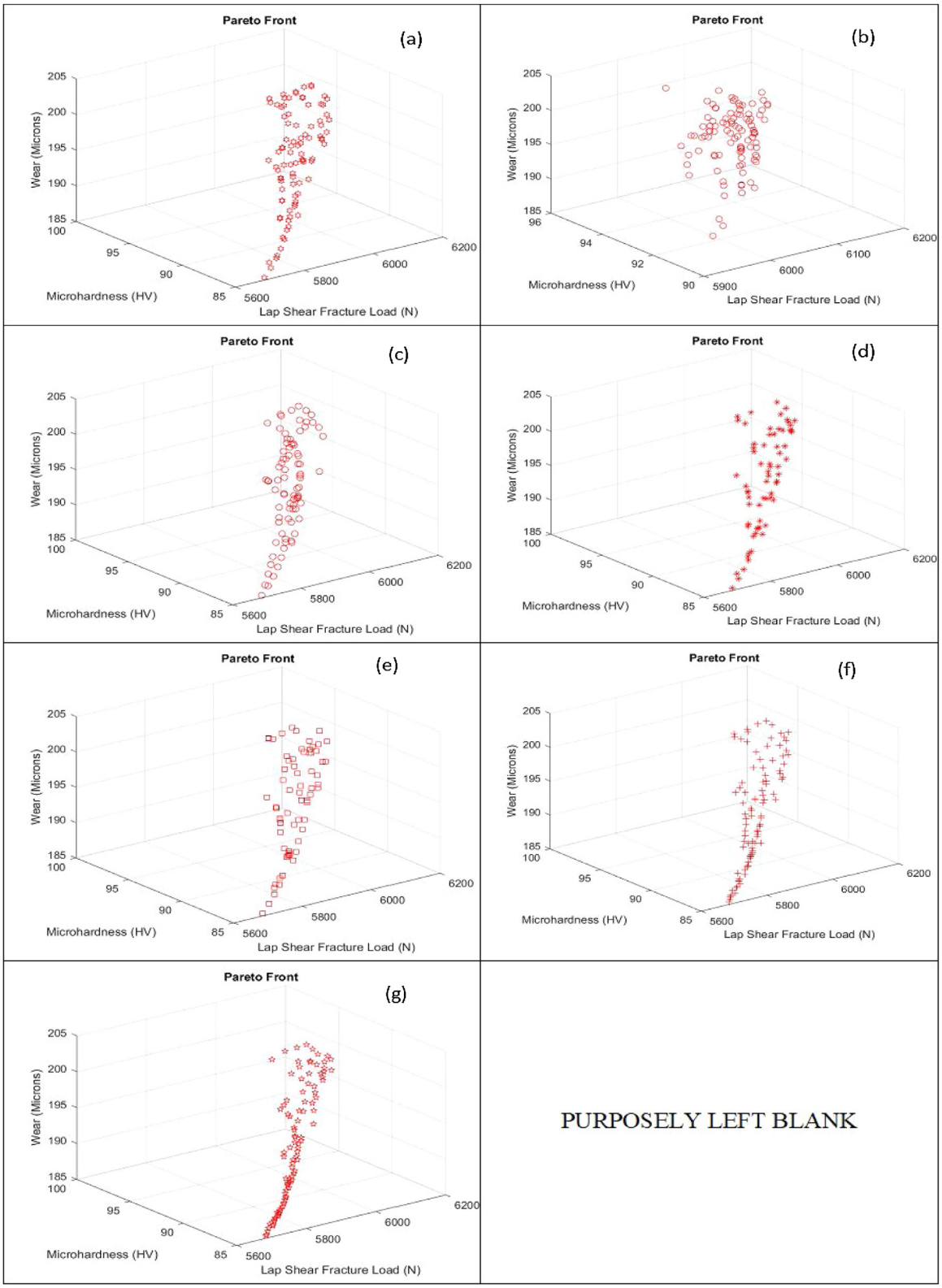

Fig. 15 – The Pareto fronts of (a) MOPSO, (b) NSGA-II, (c) MOGWO, (d) MOTLBO, (e) MO-ITLBO, (f) NSTLBO and (g) NSTLBO-MLPs.

joints during FSW or FSSW. These defects affect the mechanical properties of the weld strength. Hook formation can be quantified by height and orientation of hook [60]. Though the current study drastically improves the weld strength, the formation of keyhole was unavoidable as shown in Fig. 18(a). The refilling of the keyhole can be done using the specially

Table 10 – Wear of SFSSW joint with and without addition of Al_2O_3 nanoparticles.

Weld joint	Wear in microns	Coefficient of friction (μ)
AA6061-T6 SFSSWjoint	223	0.303
AA6061-T6/Al_2O_3 SFSSW joint	196	0.381

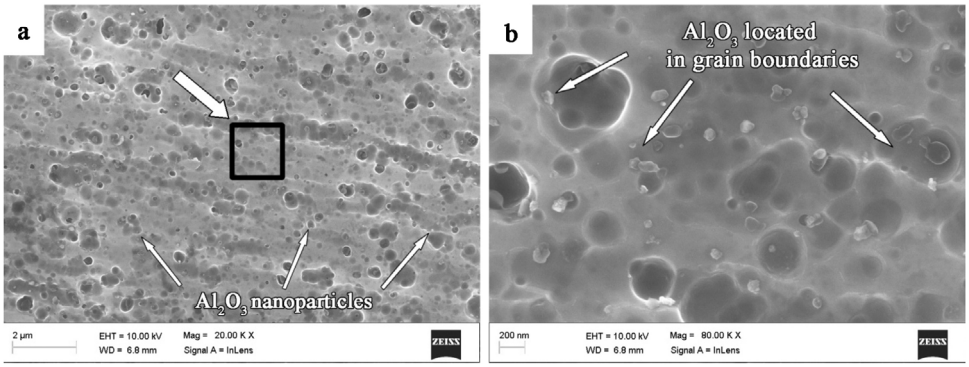

Fig. 16 – (a) FESEM images of SZ of AA6061-T6/Al_2O_3 weld joint (b) Magnified view of the portion mentioned in (a).

designed semi-consumable tool as suggested by Han et al. [61] and Zhang et al. [62].

The hook formation on weld samples with Al_2O_3 nanoparticles and without Al_2O_3 nanoparticles are shown in Fig. 18 (b) and (c). In weld joint without Al_2O_3 as shown in Fig. 18(b), the hook orientation is seen towards the keyhole that caused weaker weld joint. In Al_2O_3 added weld joint as shown in Fig. 18(c), the hook orientation is away from the keyhole that could delayed the propagation of crack and led to the greater strength. The hook height is also observed smaller in Al_2O_3 added weld joint. With these observations, it is understood that the smaller height of the hook and the orientation away from keyhole caused by the addition of Al_2O_3 supplemented the increase in weld strength.

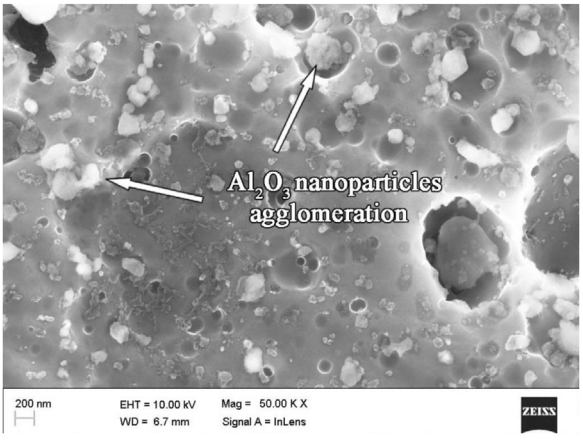

Fig. 17 – FESEM micrograph of a sample with agglomerated Al_2O_3 nanoparticle in SZ.

5.1. *FESEM fractrograph of fractured surfaces*

The SFSSW joints prepared with guide hole reinforcement and weld joints prepared with no guide hole reinforcement were examined and evaluated. Both the samples were prepared with optimal condition predicated by NSTLBO-MLPs and the mechanical tests were done as discussed in section 2.4. Fig. 19(a) and (b) show the load - displacement curve of tensile shear test and microhardness values at SZ respectively.

The lap shear load of 6145 N is observed from Al_2O_3 reinforced weld joint, while it is 4924 N for SFSSW joint with no Al_2O_3 reinforcement. The Al_2O_3 nanoparticles added joint is consistent with the larger elongation under tensile loading compared to the sample with no addition of nanoparticles as shown in Fig. 19(a). The results vividly evidence the effect of reinforcement in guide hole. Similarly, as seen in Fig. 19(b), microhardness at SZ of reinforced SFSSW joint is higher than the other one. The well distribution of Al_2O_3 nanoparticles evidenced in Fig. 16(b) supports these results. The homogeneous distribution of nanoparticles affixes the grain boundaries and delays the growth of Al grains inside the SZ. According to Hall-Petch equation, decreasing the grain size leads to strengthening of grain boundary and results higher ultimate failure load [63].

Fig. 20 shows the FESEM fractography of fractured surface of AA6061-T6/Al_2O_3 SFSSW sample during the tensile shear test. The fracture surface of the sample with the addition of Al_2O_3 nanoparticles has smaller and shallow dimples. The dimple rupture is evidenced for the ductile fracture which caused the higher tensile strength. Al_2O_3 nanoparticles are visible in the magnified image shown in Fig. 20(b). The good coherency between Al_2O_3 nanoparticles and aluminium matrix that causes narrow dimples is observed.

The maximum lap shear load obtained in the present study was compared with the failure load reported in other various spot joining process on Al alloys [64–69]. It is observed from Fig. 21 that the maximum lap shear load of Al_2O_3 reinforced weld sample prepared at optimum condition is the superior than all published works.

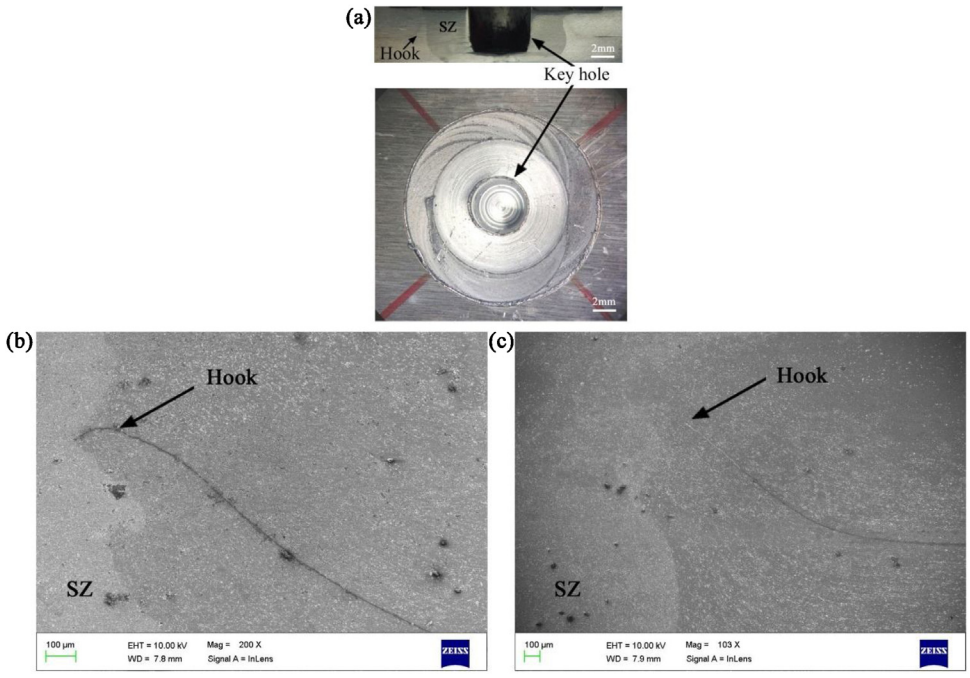

Fig. 18 – (a) Keyhole and hook defects (b) Hook orientation on weld sample without Al_2O_3 (c) Hook orientation on weld sample with Al_2O_3.

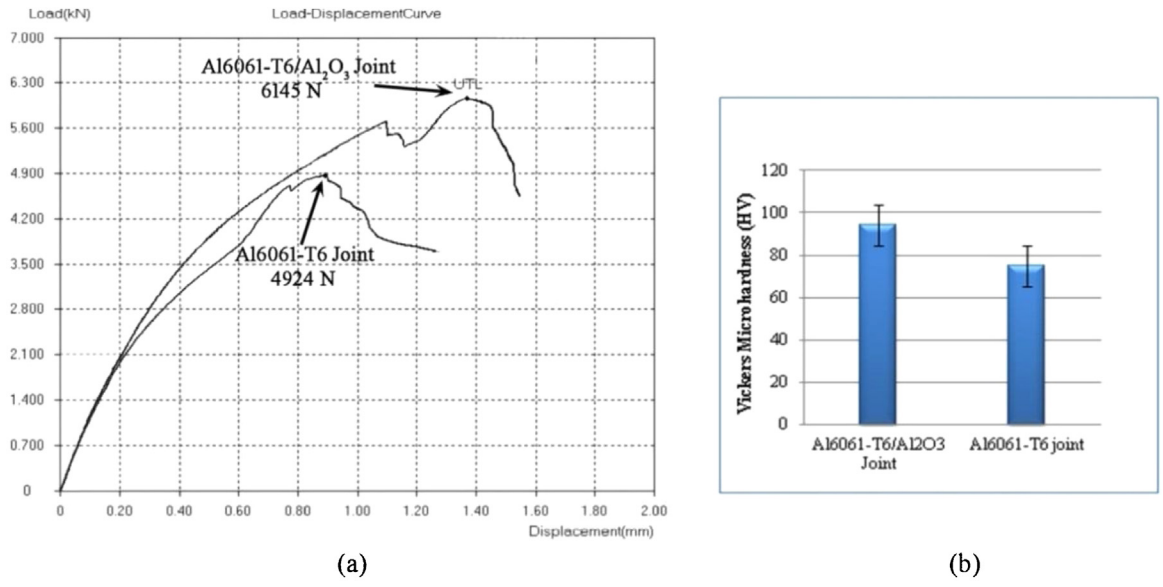

Fig. 19 – (a) Lap shear load (N) - Displacement (mm) curve of weld joints (b) Microhardness value at SZ of weld joints.

5.2. *FESEM fractrograph of worn surfaces*

Table 10 shows the results of wear in microns and coefficient of friction of SFSSW joints with and without the addition of Al_2O_3 nanoparticles, both prepared at optimal welding condition predicted by NSTLBO-MLPs. It is clearly noticed that SFSSW joint prepared with Al_2O_3 nanoparticles has very less wear (196 microns) and high coefficient of friction (0.381) compared to others. The fine size of grains and homogeneous distribution of fillers in the weld zone caused to have low wear compared to other joint prepared with no reinforcement. As per Archard's relationship the enhanced hardness increases the wear resistance of the material.

Fig. 22 shows the coefficient of friction of SFSSW joints with Al_2O_3 nanoparticles and without Al_2O_3 nanoparticles.

Fig. 23 shows FESEM images of worn surfaces of weld samples made with Al_2O_3 and without the addition of Al_2O_3 nanoparticles. The significant difference is seen between morphologies of test surfaces. The severe plastic deformation and surface layer remover are seen in the nanoparticles free sam-

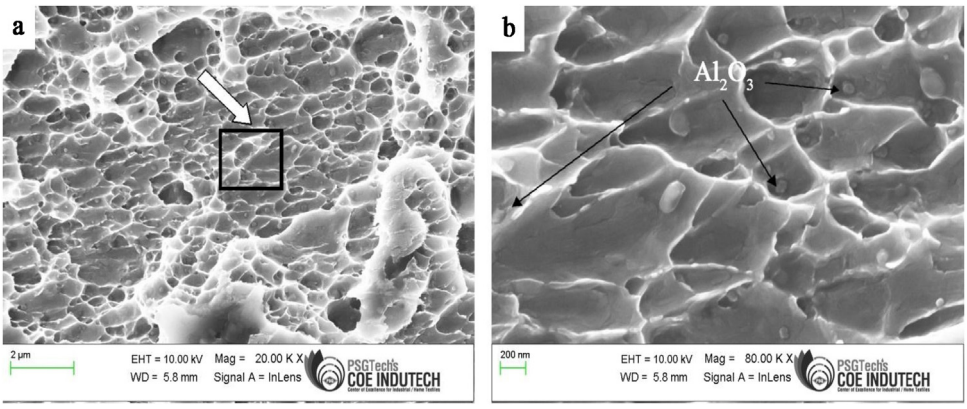

Fig. 20 – (a) FESEM fractrograph of fracture surface sample prepared at optimal condition (only the bottom sheet) (b) magnified view of portion mentioned in (a).

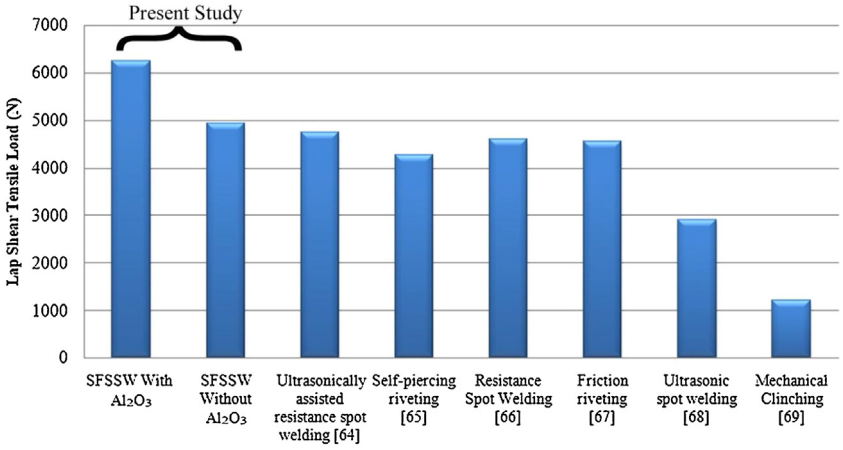

Fig. 21 – Comparison of lap shear tensile load of present research with other past researches on Al alloys.

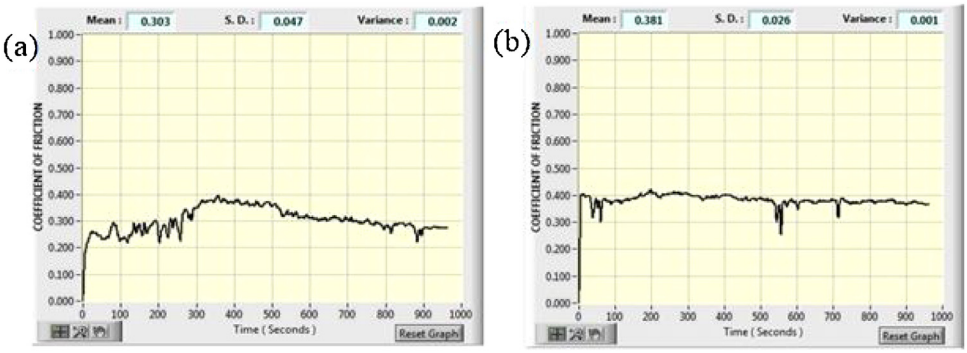

Fig. 22 – The coefficient of friction (a) AA6061-T6 SFSS weld joint (b) AA6061-T6/Al_2O_3 SFSS weld joint.

ple (Fig. 23a), which are the symbols of cruel adhesive wear mechanism [70] on the wear surfaces. However, it is observed from the morphology of worn surface of the sample with Al_2O_3 nanoparticles that it could prevent the plastic deformation and significantly reduce the material removal on the wear surface. Also observed that surface has a smooth and uniform wear morphology as shown in Fig. 23(b). The grooves are mostly restricted by uniform distribution of reinforcement.

6. Conclusions

The optimization of process parameters of SFSSW was conducted through a newly proposed NSTLBO-MLPs algorithm. SFSSW was conducted on AA6061-T6 with addition of Al_2O_3 nanoparticles into the guide holes. The response variables such as lap shear load, microhardness and wear were measured in each experiment and response surface models

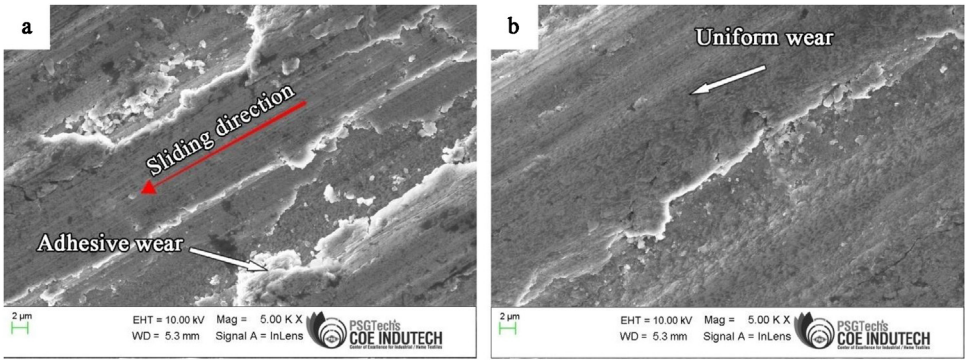

Fig. 23 – FESEM micrograph of worn surface of (a) AA6061-T6 SFSS weld joint(b) AA6061-T6/Al_2O_3 SFSS weld joint.

were developed for maximizing lap shear load and microhardness and minimizing wear. NSTLBO-MLPs optimization predicted the optimal condition as $D = 2.8$ mm, N =1387 rpm and $F = 17$ mm/minute with the predicted wear, lap shear fracture load and microhardness values of 197 microns, 6134 N and 94.6 HV, respectively. The validation experiments supported the predicted values with negligible error within 0.5 %. The proposed NSTLBO-MLPs was compared with six other metaheuristic search algorithms. The results revealed that the NSTLBO-MLPs algorithm delivers the most competitive performances by generating most uniformly distributed Pareto fronts with highest numbers of non-dominated solutions for all population sizes. Lastly, the microscopic examinations on weld samples prepared at optimal condition and fractured samples were presented and discussed. It is concluded that the reinforcement of Al_2O_3 nanoparticles into the guide holes improve the mechanical properties drastically. The proposed algorithm best predicts the optimal condition of SFSSW of AA6061-T6 alloy. The results presented in the current article do assist the industries in their production to avoid the wastage in the weld processes.

Conflict of interest

The authors declare no conflicts of interest.

Acknowledgment

This work is supported by the Fundamental Research Grant Scheme (FRGS) with project code of FRGS/1/2019/TK04/UCSI/02/1 awarded by the Ministry of Higher Education, Malaysia.

REFERENCES

[1] Singh Virendra Pratap, Patel Surendra Kumar, Ranjan Alok, Kuriachen Basil. Recent research progress in solid state friction-stir welding of aluminium–magnesium alloys: a critical review. J Mater Res Technol 2020;9(3):6217–56.
[2] Iwashuta T. Spot friction welding to achieve light weight automobile-body. Weld World 2004;48:71–7.
[3] Ojo OO, Taban E, Kaluc E. Friction stir spot welding of aluminum alloys: a recent review. Mater Test 2015;57(7-8):609–27.
[4] Haghshenas M, Gerlich AP. Joining of automotive sheet materials by friction-based welding methods: a review. Int J Eng Sci Technol 2018;21:130–48.
[5] Burford D, Tweedy B, Widener C. Fatigue crack growth in integrally stiffened panels joined using friction stir welding and swept friction stir spot welding. J ASTM Int 2008;5(4):1–18.
[6] Lakshminarayanan AK, Annamalai VE, Elangovan K. Identification of optimum friction stir spot welding process parameters controlling the properties of low carbon automotive steel joints. J Mater Res Technol 2015;4(3):262–72.
[7] Suresh S, Venkatesan K, Rajesh S. Optimization of process parameters for friction stir spot welding of AA6061/Al2O3 by Taguchi method. AIP Conf Proc 2019:2128, http://dx.doi.org/10.1063/1.5117961.
[8] Yang XW, Fu T, Li WY. Friction stir spot welding: a review on joint macro- and microstructure, property, and process modelling. Adv Mater Sci Eng 2014;2014:1–11.
[9] Li Gaohui, Li Zhoua, Zhou Weilu, Song Xiaoguo, Huang Yongxian. Influence of dwell time on microstructure evolution and mechanical properties of dissimilar friction stir spot welded aluminum–copper metals. J Mater Res Technol 2019;8(3):2613–24.
[10] Rohani Yazdi R, Beidokhti B, Haddad-Sabzevar M. Pin less tool for FSSW of AA 6061-T6 aluminum alloy. J Mater Process Technol 2019;267:44–51.
[11] Barmouz M, Givi MKB, Seyfi J. On the role of processing parameters in producing Cu/SiC metal matrix composites via friction stir processing: investigating microstructure, microhardness, wear and tensile behaviour. Mater Charact 2011;62(1):108–17.
[12] Bahrami M, Helmi N, Dehghani K, Givi MKB. Exploring the effects of SiC reinforcement incorporation on mechanical properties of friction stir welded 7075 aluminum alloy: fatigue life, impact energy, tensile strength. Mater Sci Eng A 2014;595:173–8.
[13] Tebyani SF, Dehghani K. Friction stir spot welding of interstitial free steel with incorporating silicon carbide nano powders. Int J Adv Manuf Technol 2013;79:343–50.
[14] Saeidi M, Abdi Behnagh R, Manafi B, Farahmand Nikoo M, Besharati Givi MK. Study on ultrafine-grained aluminum matrix nanocomposite joint fabricated by friction stir welding. Proc Inst Mech Eng Part L J Mater Des Appl 2016;230:311–8.
[15] Wu D, Shen J, Lv L, Wen L, Xie X. Effects of nano-SiC on the FSSW welded AZ31 magnesium alloy joints. Mater Sci Technol 2017;33:998–1003.

[16] Suresh S, Venkatesan K, Natarajan Elango. Influence of SiC nanoparticle reinforcement on FSS welded 6061T6 aluminum alloy. J Nanomater 2018;2018:1–10.
[17] Suresh S, Venkatesan K, Natarajan Elango, Rajesh S. Influence of tool rotational speed on the properties of friction stir spot welded AA7075-T6/Al2O3 composite joint. Mater Today Proc 2019;27:62–7, http://dx.doi.org/10.1016/j.matpr.2019.08.220.
[18] Su ZM, He RY, Lin PC, Dong K. Fatigue of alclad AA2024-T3 swept friction stir spot welds in cross-tension specimens. J Mater Process Technol 2016;236:162–75.
[19] Venukumar S, Yalagi S, Muthukumaran S. Comparison of microstructure and mechanical properties of conventional and refilled friction stir spot welds in AA6061-T6 using filler plate. Trans Nonferrous Met Soc China 2013;23:2833–42.
[20] Suresh S, Venkatesan K, Natarajan Elango, Rajesh S, Hong Lim Wei. Evaluating weld properties of conventional and swept friction stir spot welded 6061-T6 aluminium alloy. Mater Express 2019;9:851–60.
[21] Brown J, Burford DA, Widener CA, Horn W, Talia J, Tweedy BM. Corrosion and fatigue evaluation of swept friction stir spot welding through sealants and surface treatments. in: friction stir welding & processing V, San Francisco, California; 2009. p. 273–85.
[22] Awang M, Ismail A, Zaman MAK. Effect of process parameters on the strength of swept friction stir spot welded plates. In: Öchsner A, Altenbach H, editors. Machining, joining and modifications of advanced materials. Singapore: Springer; 2016. p. 105–10, http://dx.doi.org/10.1007/978-981-10-1082-8_11.
[23] Yoon JY, Kim C, Rhee S. Effect of circumferential tool path control on friction stir spot welding of Al/Fe dissimilar metal joint. Sci Technol Weld Join 2016;34:6–11.
[24] Huang Y, Huang T, Wan L, Meng X, Zhou L. Material flow and mechanical properties of aluminum-to-steel self-riveting friction stir lap joints. J Mater Process Technol 2019;263:129–37, http://dx.doi.org/10.1016/j.jmatprotec.2018.08.011.
[25] Huang Y, Wang J, Wan L, Meng X, Liu H, Li H. Self-riveting friction stir lap welding of aluminum alloy to steel. Mater Lett 2016;185:181–4, http://dx.doi.org/10.1016/j.matlet.2016.08.102.
[26] Muhammad Najib A, Wu Chuan Song. Evaluation of capabilities of ultrasonic vibration on the surface, electrical and mechanical behaviours of aluminium to copper dissimilar friction stir welds. Int J Mech Sci 2020, http://dx.doi.org/10.1016/j.ijmecsci.2020.105784.
[27] Rai R, De A, Bhadeshia HKDH, DebRoy T. Review: friction stir welding tools. Sci Technol Weld Join 2011;16:325–42.
[28] Ding Y, Shen Z, Gerlich AP. Refill friction stir spot welding of dissimilar aluminum alloy and AlSI coated steel. J Manuf Process 2017;30:353–60.
[29] Mukherjee I, Ray PK. A review of optimization techniques in metal cutting processes. Comput Ind Eng 2006;50(1):15–34.
[30] Lim WH, Isa NAM. Particle swarm optimization with dual-level task allocation. Eng Appl Artif Intell 2015;38:88–110.
[31] Al-Omoush AA, Alsewari AA, Alamri HS, Zamli KZ. Comprehensive review of the development of the harmony search algorithm and its applications. IEEE Access 2019;7:14233–45.
[32] Zou F, Chen D, Xu Q. A survey of teaching–learning-based optimization. Neurocomputing 2019;335:366–83.
[33] Nwobi-Okoye Hidozie Chukwuemeka, Ochieze Basil Quent, Okiy Stanley. Multi-objective optimization and modeling of age hardening process using ANN, ANFIS and genetic algorithm: results from aluminum alloy A356/cow horn particulate composite. J Mater Res Technol 2019;8(3):3054–75.
[34] Lim WH, et al. A self-adaptive topologically connected-based particle swarm optimization. IEEE Access 2018;6:65347–66.
[35] Yao L, Lim WH. Optimal purchase strategy for demand bidding. IEEE Trans Power Syst 2018;33(3):2754–62.
[36] Mukhopadhyay A, Barman KT, Sahoo P, Davim PJ. Modeling and optimization of fractal dimension in wire electrical discharge machining of EN 31 steel using the ANN-GA approach. Materials 2019;12(3):1–13.
[37] Mellal MA, Williams EJ. Parameter optimization of advanced machining processes using cuckoo optimization algorithm and hoopoe heuristic. J Intell Manuf 2016;27(5):927–42.
[38] Rao RV, Kalyankar VD. Optimization of modern machining processes using advanced optimization techniques: a review. Int J Adv Manuf Technol 2014;73(5):1159–88.
[39] Rao RV, More KC, Taler J, Ocłoń P. Multi-objective optimization of thermo-acoustic devices using teaching-learning-based optimization algorithm. Sci Technol Built Environ 2017;23(8):1244–52.
[40] Rao RV, Rai DP, Balic J. Multi-objective optimization of abrasive waterjet machining process using Jaya algorithm and PROMETHEE method. J Intell Manuf 2019;30(5):2101–27.
[41] Suresh P, Venkatesan R, Sekar T, Elango N, Sathiyamoorthy V. Optimization of intervening variables in MicroEDM of SS316L using a genetic algorithm and response-surface methodology. Strojniški vestnik – J Mech Eng 2014;60(10):9–10.
[42] Sathiyamoorthy V, Sekar T, Elango N. Optimization of processing parameters in ECM of die tool steel using nanofluid by multi objective genetic algorithm. The Scientific World Journal 2015;2015:1–6.
[43] Sathiyamoorthy V, Sekar T, Suresh P, Vijayan R, Elango N. Optimization of processing parameters in electrochemical machining of AISI 202 using response surface methodology. Int J Eng Sci Technol 2015;10(6):780–9.
[44] Teimouri R, Baseri H, Moharami R. Multi-responses optimization of ultrasonic machining process. J Intell Manuf 2015;26(4):745–53.
[45] Mohanty CP, Mahapatra SS, Singh MR. A particle swarm approach for multi-objective optimization of electrical discharge machining process. J Intell Manuf 2016;27(6):1171–90.
[46] Ong P, Chong CH, bin Rahim MZ, Lee WK, Sia CK, bin Ahmad MAH. Intelligent approach for process modelling and optimization on electrical discharge machining of polycrystalline diamond. J Intell Manuf 2018, http://dx.doi.org/10.1007/s10845-018-1443-1446.
[47] Nagarajan P, Murugesan PK, Natarajan E. Optimum control parameters during machining of LM13 aluminum alloy under dry electrical discharge machining (EDM) with a modified tool design. Mater Sci 2019;25(4).
[48] Kaviarasan V, Venkatesan R, Natarajan E. Prediction of surface quality and optimization of process parameters in drilling of Delrin using neural network. Prog Rubber Plast Recycl Technol 2019;35(3):149–69.
[49] Lin W, Yu DY Wang S, Zhang C, Zhang S, Tian H, Luo M, et al. Multi-objective teaching–learning-based optimization algorithm for reducing carbon emissions and operation time in turning operations. Eng Optim 2015;47(7):994–1007.
[50] Abhishek K, Rakesh Kumar V, Datta S, Mahapatra SS. Parametric appraisal and optimization in machining of CFRP composites by using TLBO (teaching–learning based optimization algorithm). J Intell Manuf 2017;28(8):1769–85.
[51] Rao RV, Rai DP, Balic J. Multi-objective optimization of machining and micro-machining processes using non-dominated sorting teaching–learning-based optimization algorithm. J Intell Manuf 2018;29(8):1715–37.
[52] Natarajan E, Kaviarasan V, Lim WH, Tiang SS, Tan TH. Enhanced multi-objective teaching-learning-based

optimization for machining of Delrin. IEEE Access 2018;6:51528–46.
[53] Natarajan E, Kaviarasan V, Lim WH, Tiang SS, Parasuraman S, Elango S. Non-dominated sorting modified teaching–learning-based optimization for multi-objective machining of polytetrafluoroethylene (PTFE). J Intell Manuf 2019, http://dx.doi.org/10.1007/s10845-019-01486-9.
[54] Coello CAC, Pulido GT, Lechuga MS. Handling multiple objectives with particle swarm optimization. Ieee Trans Evol Comput 2004;8(3):256–79.
[55] Deb K, Pratap A, Agarwal S, Meyarivan T. A fast and elitist multiobjective genetic algorithm: NSGA-II. Ieee Trans Evol Comput 2002;6(2):182–97.
[56] Mirjalili S, Saremi S, Mirjalili SM, Coelho LDS. Multi-objective grey wolf optimizer: a novel algorithm for multi criterion optimization. Expert Syst Appl 2016;47:106–19.
[57] Patel VK, Savsani VJ. A multi-objective improved teaching–learning based optimization algorithm (MO-ITLBO). Inf Sci (Ny) 2016;357:182–200.
[58] Darzi Bourkhani R, Eivani AR, Nateghi HR, Jafarian HR. Effects of pin diameter and number of cycles on microstructure and tensile properties of friction stir fabricated AA1050-Al2O3 nanocomposite. J Mater Res Technol 2020;9(3):4506–17.
[59] Meng X, Huang Y, Cao J, Shen J, dos Santos JF. Recent progress on control strategies for inherent issues in friction stir welding. Prog Mater Sci 2020, http://dx.doi.org/10.1016/j.pmatsci.2020.100706.
[60] Ravi KK, Narayanan RG, Rana PK. Friction stir Spot Welding of Al6082-T6/HDPE/Al6082-T6/HDPE/Al6082-T6 sandwich sheets: hook formation and lap shear test performance. J Mater Res Technol 2018;8(1):615–22, http://dx.doi.org/10.1016/j.jmrt.2018.05.011.
[61] Han B, Huang Y, Lv S, Wan L, Feng J, Fu G. AA7075 bit for repairing AA2219 keyhole by filling friction stir welding. Mater Des 2013;51:25–33, http://dx.doi.org/10.1016/j.matdes.2013.03.089.
[62] Zhang Z, Yu Y, Zhao H, Wang X. Interface behavior and impact properties of dissimilar Al/Steel keyhole-free FSSW joints. Metals 2019;9(6):691, http://dx.doi.org/10.3390/met9060691.
[63] Paidar M, Vaira Vignesh R, Khorram A, Oladimeji Ojo O, Rasoulpouraghdam A, Pustokhina I. Dissimilar modified friction stir clinching of AA2024-AA6061 aluminum alloys: effects of materials positioning. J Mater Res Technol 2020;9(3):6037–47.
[64] Shah U, Liu X. Effect of ultrasonic energy on the spot weldability of aluminum alloy AA60601. Mater Des 2020:108690, http://dx.doi.org/10.1016/j.matdes.2020.108690.
[65] Hoang NH, Porcaro R, Langseth M, Hanssen AG. Self-piercing riveting connections using aluminium rivets. Int J Solids Struct 2010;47(3-4):427–39, http://dx.doi.org/10.1016/j.ijsolstr.2009.10.009.
[66] Li Y, Yan F, Luo Z, Chao YJ, Ao S, Cui X. Weld growth mechanisms and failure behavior of three-sheet resistance spot welds made of 5052 aluminum alloy. J Mater Eng Perform 2015;24(6):2546–55, http://dx.doi.org/10.1007/s11665-015-1519-9.
[67] Cordeiro de Proença B, Blaga L, Fernandez dos Santos J, Bresciani Canto L, de Traglia Amancio Filho S. Friction riveting ("FricRiveting") of 6056 T6 aluminium alloy and polyamide 6: influence of rotational speed on the formation of the anchoring zone and on mechanical performance. Weld Int 2017;31(7):509–18, http://dx.doi.org/10.1080/09507116.2016.1218627.
[68] Rajalingam P, Rajakumar S, Balasubramanian V, Kavitha S, Raja Muthamil Selvan M. Exploratory study on the effect of amplitude on ultrasonic spot welding of aerospace materials. Mater Today Proc 2020, http://dx.doi.org/10.1016/j.matpr.2020.02.811.
[69] Lambiase F, Paoletti A, Di Ilio A. Advances in mechanical clinching: employment of a rotating tool. Procedia Eng 2017;183:200–5, http://dx.doi.org/10.1016/j.proeng.2017.04.021.
[70] Liu W, Yan H, Zhu JB. Effect of the addition of rare earth element La on the tribological behaviour of AlSi5Cu1Mg alloy. Appl Sci 2018;8(2), http://dx.doi.org/10.3390/app8020163.